Oxygen isotope analysis of the eyes of pelagic trilobites: testing the application of sea temperature proxies for the Ordovician

Bennett, Carys E. [1,2*], Williams, Mark[2], Leng, Melanie J.[3], Lee, Martin, R.[4], Bonifacie, Magali[5,6], Calmels, Damien[5,7], Fortey, Richard A.[8], Laurie, John R.[9], Owen, Alan W.[4], Page, Alex A.[2], Munnecke, Axel[10], Vandenbroucke, Thijs R. A.[1,11]

[1] Evo-Eco-Paleo, UMR 8198 du CNRS, Université Lille 1, Avenue Paul Langevin, bâtiment SN5, 59655 Villeneuve d'Ascq cedex, France.

[2]School of Geography, Geology and the Environment, University of Leicester, University Road, Leicester, LE1 7RH, UK.

[3] NERC Isotope Geosciences Laboratory, British Geological Survey, Keyworth, Nottingham, NG12 5GG, UK and Centre for Environmental Geochemistry, School of Biosciences, Sutton Bonington Campus, University of Nottingham, Loughborough, LE12 5RD, UK.

[4]School of Geographical & Earth Sciences, University of Glasgow, Gregory Building, Lilybank Gardens, Glasgow, G12 8QQ, UK.

[5]Institut de Physique du Globe de Paris, Equipe Géochimie des Isotopes Stables, Sorbonne Paris Cité, Univ Paris Diderot, UMR 7154 CNRS, F-75005 Paris, France.

[6]Institut de Physique du Globe de Paris, Observatoire Volcanologique et Sismologique de Guadeloupe, Le Houëlmont, 97113 Gourbeyre Guadeloupe, France.

[7]Université Paris-Sud, Laboratoire GEOPS, UMR 8148 CNRS, F-91405 Orsay, France.

[8]The Natural History Museum, Cromwell Road, London SW7 5BD, UK.

[9]Department of Biological Sciences, Macquarie University, NSW 2109, Australia.

[10]Universität Erlangen-Nürnberg, GeoZentrum Nordbayern, Fachgruppe Paläoumwelt, Loewenichstrasse 28, D – 91054, Erlangen, Germany.

[11]Department of Geology, Ghent University, Krijgslaan 281/S8, 9000 Ghent, Belgium.

*e-mail: ceb28@le.ac.uk

Research Highlights

1. Preservation assessment shows some well-preserved Ordovician trilobite eyes
2. Ordovician trilobite eyes yield $\delta^{18}O$ values similar to Ordovician brachiopods
3. SIMS and clumped isotope results indicate diagenetic alteration of trilobites
4. Classic protocols to assess preservation may be inapt for most ancient carbonates

Abstract

The oxygen isotope composition of well-preserved trilobite eye calcite, retaining its original optical properties, represents a possible source of information on Paleozoic sea temperatures. Species of the epipelagic telephinid genera *Carolinites* and *Opipeuterella* from strata of Early to Middle Ordovician age in Spitsbergen and Australia were analyzed, and compared with benthic asaphid species. Scanning electron microscope (SEM), cathodoluminescence (CL), electron microprobe and Electron Backscatter Diffraction (EBSD) techniques were used to assess eye preservation prior to isotope analysis. Some apparently well-preserved eyes are identified from the Valhallfonna (Spitsbergen) and Emanuel (Australia) formations. The eyes show a wide variation in $\delta^{18}O$ values: –6.2‰ to –9.8‰ for the Valhallfonna Formation, –3.2‰ to –10.4‰ for the Emanuel Formation, and –3.6‰ to –7.4‰ for the Horn Valley Siltstone (Australia). Intra-eye Secondary Ion Mass Spectrometry (SIMS) isotope results reveal an even larger range in $\delta^{18}O$ in some specimens ($\delta^{18}O$ of –2.4‰ to –10.4‰), suggesting that the trilobite eyes have undergone cryptic recrystallization. A sub-set of trilobite cuticle from the three formations were analyzed for their carbonate clumped isotope compositions (Δ_{47}), and yielded crystallisation temperatures above 50°C, consistent with diagenetic alteration. The SIMS and Δ_{47} results suggest that classic preservation assessment protocols for the stable isotope study of deep-time carbonate samples may be insufficient, especially for these techniques. There is a need for extensive microstructural characterisation of lower Paleozoic biogenic carbonates, by techniques including EBSD, SIMS and Δ_{47}, before their stable isotope signatures can be used with certainty in paleoclimate studies.

Index terms: Stable isotope geochemistry; marine geochemistry; instruments and techniques; biomineralization; petrography, microstructures, and textures

Keywords: Trilobite, oxygen isotopes, Ordovician, paleotemperature, microstructure

1. Introduction

Telephinid trilobites are amongst the few unequivocally pelagic organisms preserved in Ordovician rocks that have a carbonate biomineralized skeleton. The most common telephinid, *Carolinites genacinaca*, had a global paleoequatorial distribution during the Early Ordovician (Floian) and the morphology of the *Carolinites* body plan, eye shape and eye position suggest that species were epipelagic, living near the sea surface in the mixed layer (McCormick and Fortey, 1998, 1999). The holochroal eyes of telephinid trilobites are composed of hundreds of interlocking lenses of calcite and are sufficiently large to provide sufficient material for stable isotope analysis, which in turn might conceivably yield an estimate of Ordovician sea temperature.

Trilobite cuticle has been used in Ordovician isotope paleoclimate studies in the same way as brachiopod calcite (Brand, 2004; Finnegan et al., 2011). Studies on the ultrastructure of the biomineralized trilobite exoskeleton (the cuticle) show that original features such as horizontal lamination, relict organic material, and pore canals can be preserved (Dalingwater, 1973; Dalingwater et al., 1991), although evidence for diagenetic alteration is also common (Wilmot, 1990; Budil and Hörbinger, 2007). Investigations into the original chemical and isotope compositions of trilobite cuticles indicate that they were formed from low-Mg calcite (Wilmot and Fallick, 1989; Lee et al., 2012; McRoberts et al., 2013; Teigler and Towe, 1975). Some specimens have been recorded with an intermediate-Mg calcite composition (Brand, 2004; McAlister and Brand, 1989). However, as the preservation of the cuticle ultrastructure in these latter specimens was not examined in detail, the possibility remains that the chemical composition of these cuticles may reflect diagenetic recrystallization in Mg-rich fluid. The lenses in the schizochroal eyes of phacopine trilobites have

been identified as being originally composed of high-Mg calcite of ~7.5 mol% $MgCO_3$, while the cuticle comprises low-Mg calcite of ~1.4 to 2.4 mol% $MgCO_3$ (Lee et al., 2012).

As the physical properties of a functional calcite lens are well understood, even if trilobite eyes do not have modern analogues, it is possible to assess their degree of preservation (Torney et al., 2014). Previous work on the ultrastructure of schizochroal trilobite eyes using EBSD has revealed that the original structure of the eye lenses can be identified (Lee et al., 2007, 2012; Torney et al., 2014). This finding suggests the possibility that the original chemical and isotope composition of eye calcite may also be retained. High-resolution SEM analysis of the lenses of phacopine trilobite eyes show that the intralensar bowl (present only in schizochroal eyes) was composed of high-Mg calcite with micro-crystals of dolomite indicating diagenetic alteration (Lee et al., 2007; 2012). SIMS analysis can be used to target small (less than 20 μm diameter) areas of a fossil *in situ*, such as trilobite eye lenses, and SIMS analysis of $\delta^{18}O$ has been successfully applied to the analysis of conodont microfossils (Wheeley et al., 2012).

Biogenic proxies that have been hitherto used to provide Early and Middle Ordovician marine paleotemperatures are the oxygen isotopic compositions of brachiopod calcite and conodont apatite (Shields et al., 2003; Trotter et al., 2008; Wadleigh and Veizer, 1992), along with carbonate clumped isotope compositions (Δ_{47}) from trilobite, brachiopod and coral calcite for the Late Ordovician (Finnegan et al., 2011). However, some of these results are controversial. For instance, brachiopod isotope data from the Lower Ordovician can have very low $\delta^{18}O$ (down to –10‰). This result implies very high (up to + 60°C) seawater temperatures [if it is assumed that seawater $\delta^{18}O$ was similar to today], or diagenetic alteration at higher temperatures than that of the ocean, diagenetic alteration by a different fluid, or that seawater $\delta^{18}O$ was substantially different from present (Veizer et al., 1999; Shields et al., 2003), or a combination of those alternatives. In contrast, $\delta^{18}O$ from conodont apatite from the Ordovician suggests that seawater temperatures were between 30-40°C if a value similar to modern $\delta^{18}O_{water}$ of –1‰$_{VSMOW}$ is used (Trotter et al., 2008). Oxygen isotope data can also reflect other environmental parameters; for example, Bickert et al.

(1997) showed that the $\delta^{18}O$ values of well-preserved Silurian brachiopods reflect salinity differences due to varying fresh-water input rather than temperatures. Nevertheless, the development of proxies that can provide robust and reasonable estimates of seawater temperature for the early Paleozoic is important for many reasons. For example, such information can help constrain the environmental feedbacks or triggers of the Great Ordovician Biodiversification Event (Trotter et al., 2008; Amberg et al., 2016), and it also represents one of the few available proxies for ground-truthing General Circulation Models of early Paleozoic climate (Vandenbroucke et al., 2009; Pohl et al., 2014; 2016). Changes in seawater temperatures may have had significant effects on the ability of organisms to biomineralize (Pruss et al., 2010). The Δ_{47} paleothermometer has great potential for more accurate paleotemperature reconstruction because it is independent of the $\delta^{18}O$ of mineralising fluids (Ghosh et al., 2006). Usefully, the recrystallization temperature of diagenetic calcite recorded by Δ_{47} is thought to remain stable over hundreds of millions of years, at temperature histories below ~250ºC (Ghosh et al., 2006). However, in deeply buried sedimentary deposits or carbonates having a moderate-temperature burial history (~100°C on timescales of hundreds of million years) the closed-system solid-state diffusive reordering of atoms can modify Δ_{47} towards lower values and higher apparent equilibrium temperatures (Passey and Henkes, 2012; Henkes et al., 2014; Stolper and Eiler, 2015).

Here we test whether: (i) the unique functional morphology and microstructure of trilobite eyes allows for the accurate assessment of the preservation of their calcite lenses; and (ii) the subsequent $\delta^{18}O$ analyses of well-preserved eyes of epipelagic trilobites could serve as a sea temperature proxy. Trilobite eye microstructure and composition were compared to those of the trilobite cuticle. Two isotope methods were used on trilobite material from three sedimentary formations considered to have experienced relatively limited diagenesis: (i) conventional determination of oxygen isotope compositions, and (ii) carbonate clumped isotope Δ_{47} analysis.

2. Materials Utilised

Trilobite eyes were analyzed from three broadly coeval Ordovician formations from separate, equatorial basins: 1) Valhallfonna Formation, Spitsbergen; 2) Emanuel Formation, Canning Basin, Australia; and 3) Horn Valley Siltstone, Amadeus Basin, Australia (Figure 1). For all formations, the following materials were analyzed for $\delta^{18}O$, $\delta^{13}C$ and clumped isotope Δ_{47} compositions, where possible: pelagic and benthic trilobite eyes and cuticle, sedimentary carbonate (host rock) and coarsely crystalline diagenetic calcite cement (spar). For comparison, additional trilobite cuticle was analyzed from the Upper Member of the Dalby Limestone of Västergötland, Sweden, as this basin has experienced significantly higher burial temperatures. The Supplementary Material (extended version) details further the type and number of analyses from each formation.

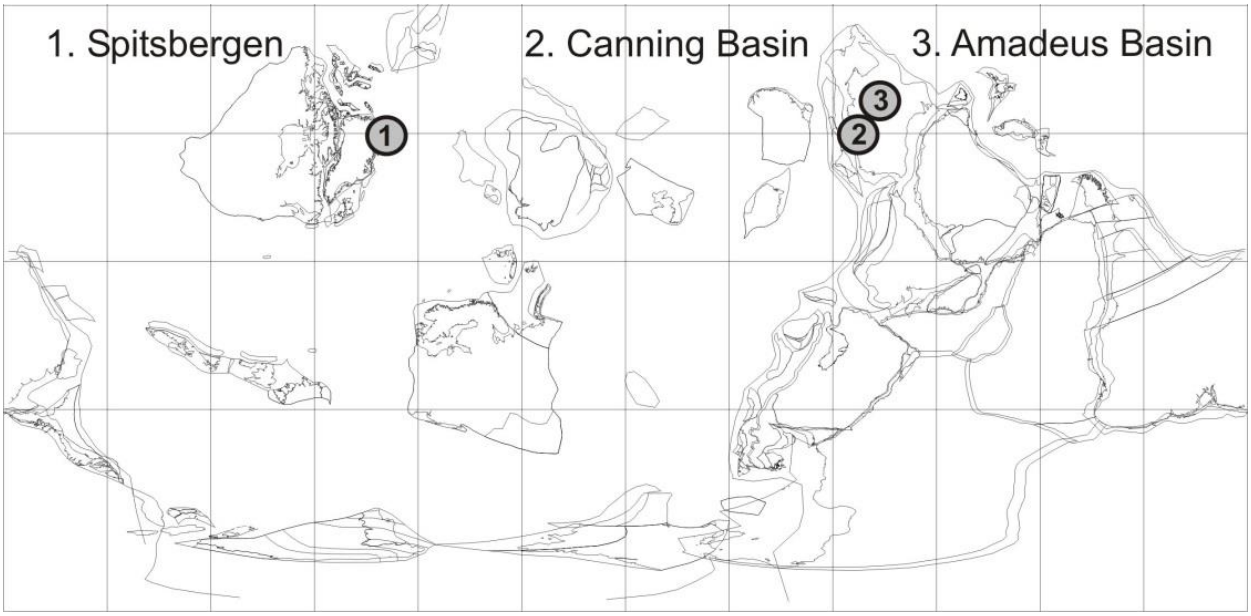

Figure 1. Paleogeographical map of trilobite sample sites: 1) Spitsbergen, Norway (Valhallfonna Formation); 2) Canning Basin, Western Australia (Emanuel Formation); and 3) Amadeus Basin, Northern Territory, Australia (Horn Valley Siltstone). Paleogeographic reconstruction for the Middle Ordovician, 470Ma, Galls Projection, cropped at latitude 30°N, BugPlates: www.geodynamics.no.

2.1 Valhallfonna Formation

Forty-three trilobite eyes were examined from eleven samples collected from the Floian (Arenigian) Valhallfonna Formation of Ny Friesland, Spitsbergen (Fortey, 1975; Fortey and Bruton, 1973). Four species of the telephinid *Carolinites* were studied (*C. angustagena, C. genacinaca, C. nevadensis* and *C. sibiricus*), along with cuticle (but no eyes) from benthic olenids (species indeterminate). The depositional environment is interpreted to be a marine shelf setting (Fortey and Barnes, 1977). The Ny Friesland succession is thought to have undergone shallow burial, with Conodont Alteration Index (CAI) values of 1 suggesting maximum temperatures of 90ºC (Bergström, 1980). Calcite veins and calcite spar cements within the cavities of ostracod fossils and in pore spaces in the limestone indicate evidence for some diagenetic alteration.

2.2 Emanuel Formation

Trilobites were studied from the Floian (Bendigonian) Emanuel Formation of the Canning Basin, Western Australia (Laurie and Shergold, 1996). Fifty-one trilobite eyes were examined from the telephinid *Opipeuterella* sp. and benthic asaphids (species indeterminate), occurring in five samples from the type section of the Emanuel Formation. The burial history of the Ordovician Canning Basin indicates low thermal maturation, with a CAI index of 1 (Nicoll et al., 1993) and Apatite Fission Track Analysis (AFTA) indicating temperatures of ~100ºC during the Late Devonian/Early Carboniferous (Arne et al., 1989).

2.3 Horn Valley Siltstone

Trilobites were studied from the Floian to Dapignian (Bendigonian to Yapeenian) Horn Valley Siltstone of the Amadeus Basin, Northern Territory, Australia, which can be partly correlated to the upper part of the Emanuel Formation from the Canning Basin (Laurie, 2006). Over 100 trilobite eyes from *Carolinites genacinaca* and benthic asaphids (species indeterminate) were examined from three samples collected from a field section at Mt Olifent (fig. 6 in Laurie, 2006). The burial history for the Amadeus Basin has been determined by AFTA and organic maturity data that indicate maximum burial during the Late Carboniferous, with Ordovician strata subjected to maximum temperatures of 140ºC (Gibson et al., 2007).

2.4 Västergötland

Two test samples of *Telephina* cuticle and its host rock were analyzed for Δ_{47} from the Upper Member of the Dalby Limestone, Sandbian (Late Ordovician), in Västergötland, Sweden, introducing contrasting data from the opposite end of the preservation spectrum. The Västergötland rocks have been heated by local Permian intrusions, giving CAI values of 6 to 7 and temperatures of over 300^{o}C (Bergström, 1980).

3. Methods

3.1 Preservation Assessment Protocol

In total, 198 trilobite eyes were examined under reflected light using a binocular microscope and by SEM, which allowed an initial assessment of eye lens integrity and preservation. Of these, 34 specimens representing a range of preservation states were selected for thin section analysis, based on the eye size (greater than 1.8 mm length), to enable a detailed preservation assessment. Polished thin sections were examined by cathodoluminescence (CL) microscopy and the geochemical variation in eye specimens was quantified using electron microprobe facilities at the universities of Lille (France) and Leicester (UK). Trilobite eye specimens were imaged by SEM under high vacuum using Secondary Electron and Back Scattered Electron detectors. Electron Backscatter Diffraction (EBSD) analysis of polished thin sections was undertaken at the University of Glasgow to examine intra-lens variations in crystallographic orientations (Torney et al., 2014).

3.2 Isotope Analyses

A total of 182 isotope analyses were undertaken on trilobite eyes, cuticle and host rock from all three formations (Appendix C). $\delta^{18}O$, $\delta^{13}C$ and Δ_{47} analyses were performed using three methods: 1. Conventional isotope analysis of carbonate powder, with lens/cuticle extraction using both a hand-held dental drill and automated micro-mill, at the British Geological Survey and at the University of Erlangen, Germany; 2. Secondary Ion Mass Spectrometry (SIMS) analysis of 15 μm diameter areas of thin sections (Figure 2) at

the Centre de Recherches Pétrographiques et Géochimiques (CRPG-CNRS) facility in Nancy, France; 3. Clumped isotope analysis (Δ_{47}) and $\delta^{18}O$ and $\delta^{13}C$ analysis of carbonate powder at the Institut de Physique du Globe de Paris (IPGP, Stable Isotope team). The extraction of material by dental drill is subject to human error and samples likely contain some underlying sediment matrix material. Micro-mill extraction is accurate to an error of ~ 5 μm, however it is possible that underlying sediment is sometimes sampled. SIMS analysis is the preferred technique in this context because it can accurately sample intra-lens material from thin sections. For a more detailed account of the methods, refer to the Supplementary Methods (extended version) section.

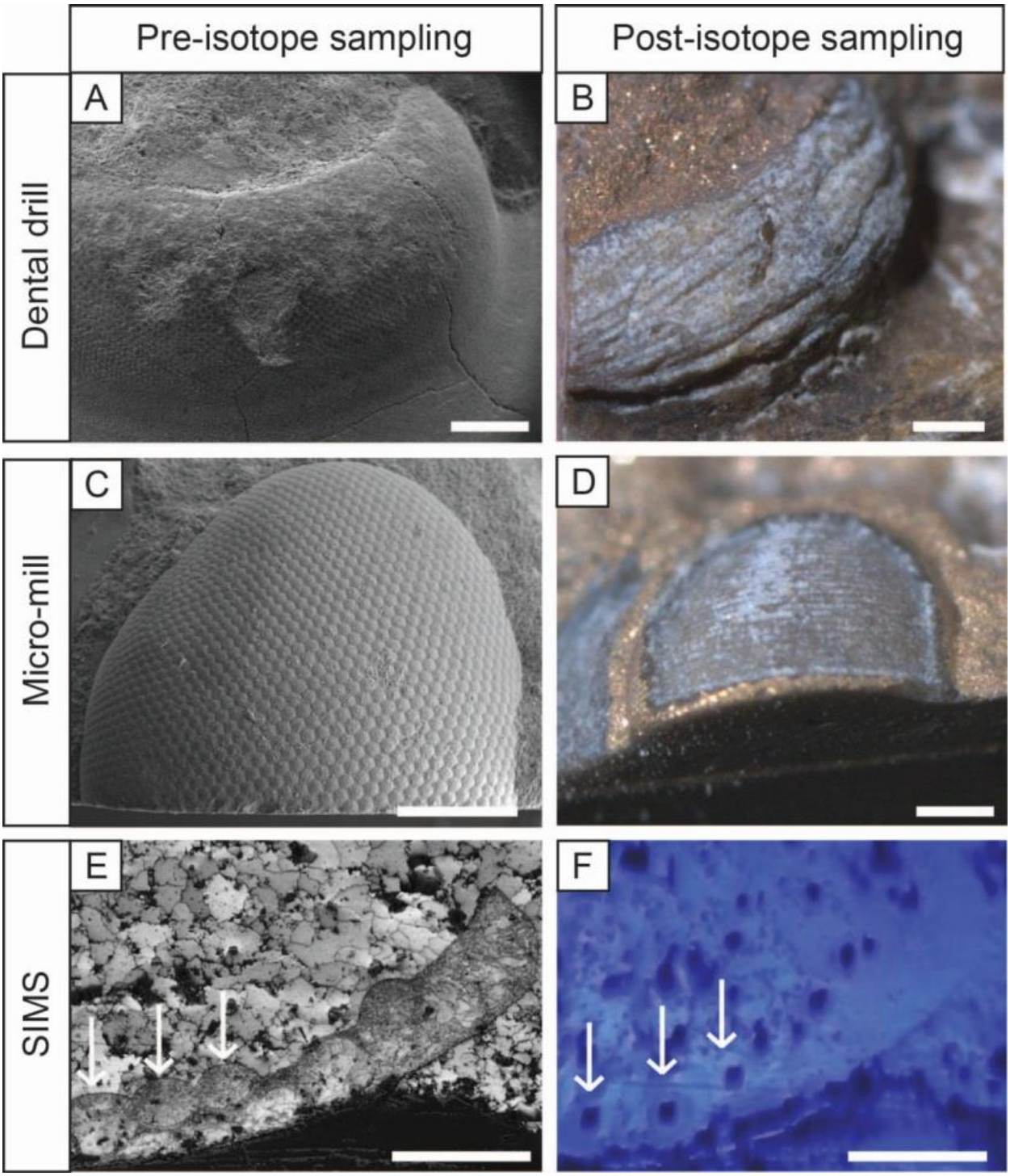

Figure 2. Lens extraction methods for isotope analysis. A-B) Hand drilling of lenses using a dentist drill for conventional isotope analysis (specimen HV_sp2, SE and light microscope images, respectively); C-D) Micro-mill automated drilling for conventional isotope analysis (specimen T_178_sp10, SE and light microscope images, respectively); E-F) Secondary Ion Mass Spectrometry (SIMS) analysis of a well-preserved eye (specimen A_178_sp1, EBSD image quality map and light microscope image, respectively).

Arrows indicate examples of lenses that were analyzed for oxygen isotopes. Scale bars 500 μm (A-D) and 100 μm (E-F).

4. Results

4.1 Preservation

The majority of the trilobite eyes examined had intact lenses that look superficially well-preserved. The hexagonal lenses are arranged in a single layer, which is on average 70 μm in thickness. Individual eye lenses are on average 50 μm in diameter, with no mineral partitions between them. Lens size varies between species, with telephinids having significantly larger lenses than asaphids, and moreover, a different eye morphology. Here we describe the results of the preservation assessment protocol from 34 specimens examined in thin section. Specimens are classified as ‘well-preserved’ or ‘poorly preserved’ based on their microstructural and geochemical properties (Table 1).

1 Table 1. Trilobite eye preservation

Specimen	Trilobite Species	CL	SEM Observations	EBSD Observations	Preservation
			Valhallfonna Formation, Spitsbergen		
1.1A_sp1	*Carolinites sibiricus*	n/a	lenses fractured, silicified	n/a	poor
1.1B_sp1	*Carolinites sibiricus*	L	pervasive porosity, recrystallized, lens boundary overgrowths	lenses undefined, major recrystallization	poor
1.1B_sp2	*Carolinites sibiricus*	L	pervasive porosity, recrystallized, fractured lenses	no lens boundaries preserved, major recrystallization	poor
1.2C_sp1	*Carolinites genacinaca*	L	pervasive porosity, recrystallized, zoned calcite, micro-dolomite	lenses defined, major recrystallization	poor
1.2C_sp2	*Carolinites genacinaca*	L	pervasive porosity, recrystallized, zoned calcite, micro-dolomite	lenses undefined, major recrystallization	poor
2.1B_sp1	*Carolinites genacinaca*	NL	lenses defined, no apparent recrystallization	lenses defined, minor recrystallization, trabeculae?	good
2.1B_sp2	*Carolinites genacinaca*	SL-L	pervasive porosity, recrystallized, micro-dolomite crystals	lenses defined, recrystallized internally, trabeculae	poor
2.6_sp1	*Carolinites angustagena*	NL	recrystallized, large crystals of dolomite, euhedral pyrite	n/a	poor
2.6_sp2	*Carolinites angustagena*	NL-L	recrystallized, zoned calcite-dolomite	n/a	poor
2.6_sp3	*Carolinites angustagena*	L	recrystallized, zoned calcite-dolomite, euhedral pyrite	n/a	poor
2.6_sp4	*Carolinites angustagena*	NL-L	recrystallized, calcite-dolomite, euhedral pyrite	n/a	poor
			Emanuel Formation, Canning Basin, Australia		
T_178_sp1	*Opipeuterella* sp.	NL	lenses defined, no apparent recrystallization	lenses defined, minor recrystallization at base of lenses	good
T_178_sp3	*Opipeuterella* sp.	L	lenses defined, crystal zoning in centre of lenses	lenses defined, minor recrystallization at lens boundaries	poor
T_178_sp4	*Opipeuterella* sp.	L	lenses defined, crystal zoning in centre of lenses	lenses defined, minor recrystallization	poor
T_178_sp10	*Opipeuterella* sp.	NL	lenses defined, pervasive porosity, micro-dolomite crystals	lenses defined, minor recrystallization, trabeculae	good
T_205_sp3	*Opipeuterella* sp.	NL	lenses defined, pervasive porosity, micro-dolomite crystals	lenses defined, minor recrystallization at cornea, trabeculae	good
T_205_sp5	*Opipeuterella* sp.	L	recrystallized, fractured lenses	n/a	poor
A_159_sp1	Asaphid indet.	NL	lenses defined, pervasive porosity, micro-dolomite crystals	lenses defined, minor recrystallization, trabeculae	good
A_159_sp4	Asaphid indet.	SL	lenses defined, no apparent recrystallization	n/a	good
A_178_sp1	Asaphid indet.	NL	lenses poorly defined, internal porosity	lenses defined, trabeculae, cuticle recrystallized	good
A_205_sp1	Asaphid indet.	NL	lenses defined, pervasive porosity, micro-dolomite crystals	lenses defined, minor recrystallization, trabeculae	good
A_205_sp3	Asaphid indet.	NL	recrystallized, lens boundaries poorly defined	lenses undefined, recrystallized	poor
A_205_sp5	Asaphid indet.	NL	lenses defined, pervasive porosity, micro-dolomite crystals	lenses defined, minor recrystallization, trabeculae	good
A_205_sp10	Asaphid indet.	NL	lenses defined, pervasive porosity, micro-dolomite crystals	lenses defined, minor recrystallization	good
			Horn Valley Siltstone, Amadeus Basin, Australia		
HV_sp2	Asaphid indet.	L	lenses distinct, recrystallized	lenses defined, calcite twinning across all lenses	poor
HV_sp4	*Carolinites genacinaca*	SL-L	lenses undefined, recrystallized, euhedral pyrite within lenses	lenses defined, major recrystallization	poor
HV_sp5	*Carolinites genacinaca*	SL	lenses undefined, some recrystallization, pyrite within lenses	lenses defined, major recrystallization	poor
HV_sp6	Asaphid indet.	L	lenses fractured, partly recrystallized, pyrite within lenses	lenses undefined, recrystallization, calcite twinning	poor
HV_sp20	Asaphid indet.	L	lenses defined, partly recrystallized, pyrite within lenses	lenses defined, calcite twinning across all lenses	poor
HV_sp27	Asaphid indet.	L	lenses undefined, recrystallized, internal porosity	no lens boundaries preserved, major recrystallization	poor
HV_sp37	*Carolinites genacinaca*	NL	lenses undefined, recrystallization, euhedral pyrite within lenses	lenses defined, recrystallization, calcite twinning	poor

HV_sp43	*Carolinites genacinaca*	SL-L	lenses defined, porosity and crystal zoning within lenses	lenses defined, recrystallization, calcite twinning	poor
HV_sp94	*Carolinites genacinaca*	SL-L	lenses defined, crystal zoning and pyrite within lenses	lenses undefined, major recrystallization	poor

Trilobite eye preservation assessment data table, for specimens examined in polished thin section. Some specimens were not observed under EBSD due to their lenses being heavily dolomitised, silicified, or fractured/broken. Note that only specimens from the Valhallfonna Formation were analyzed on the electron microprobe (see Appendix 1). Abbreviations: CL = cathodoluminescence; L = luminescent; NL = non-luminescent, SL = slightly luminescent; SEM = Scanning Electron Microscope; EBSD = Electron back scatter diffraction.

Well-preserved lenses are composed of a single calcite crystal, which is non-luminescent. The outer 1-2 μm of the lens surface consists of the cornea, which is micro-crystalline (Figure 3B) and luminescent. EBSD maps show that calcite had a uniform crystallographic orientation within each lens, with the c-axis of the calcite parallel to the lens axis (Figure 3D). Micro-scale pitting (Figure 3C) and sub-crystal boundaries (Figure 3D) are observed in some lenses. In some specimens the lenses contain trabeculae, which are microcrystallites oriented perpendicular to the lens surface and are thought to be an original structure (Clarkson et al., 2006; Schoenemann and Clarkson 2011). The trabeculae can also be seen in SEM images of broken lens sections, and can be identified in EBSD maps by slight differences in the crystallographic orientations of the constituent sub-crystals (Figure 3E). Apparently syntaxial calcite cements occur next to the interior lens surface of some specimens, but EBSD shows these cements have a different crystallographic orientation to the lens calcite.

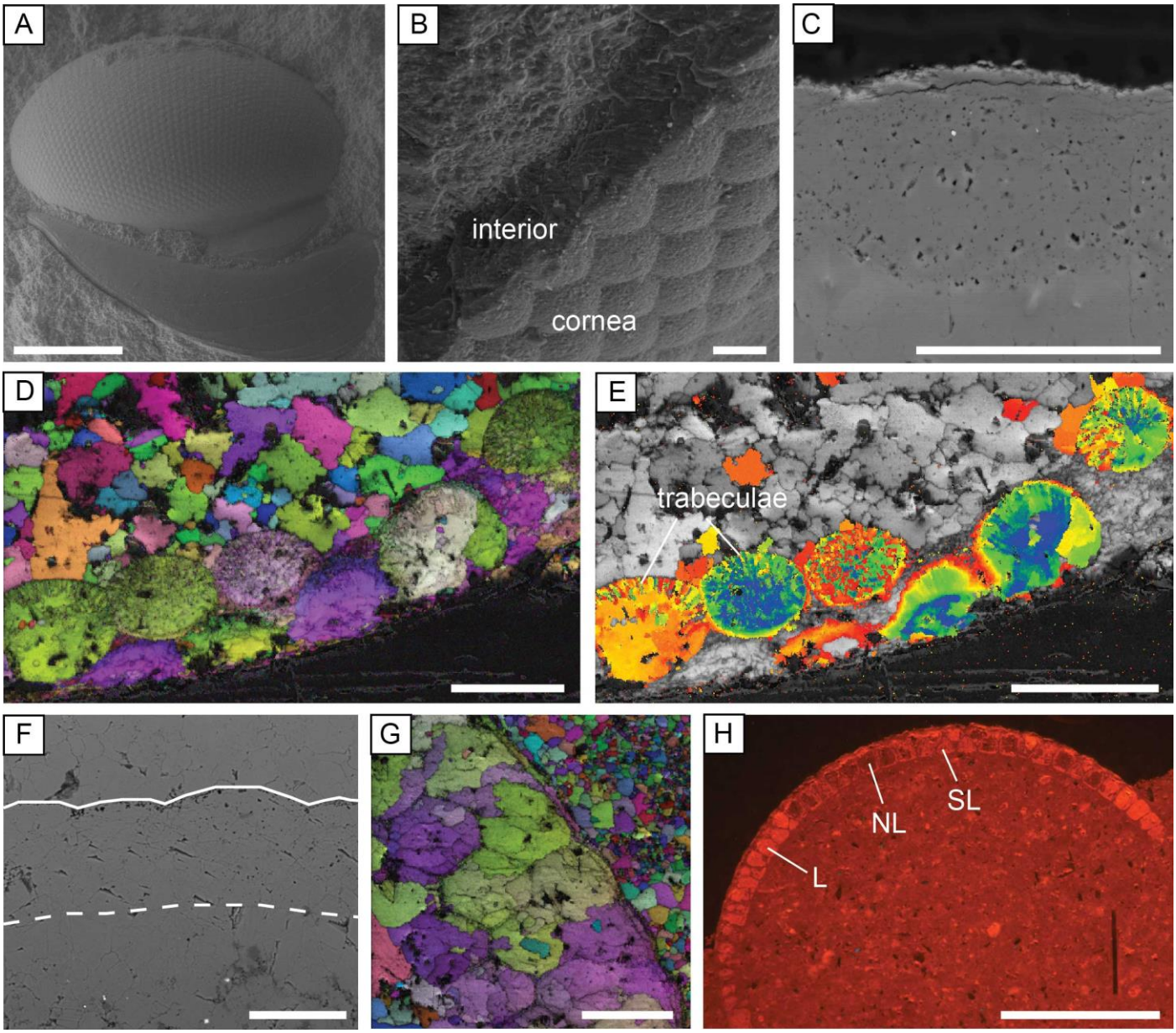

Figure 3. Trilobite eye preservation. A: *Opipeuterella* sp., with intact lenses and libriginal cuticle (specimen T_205_sp4, SE image). B: The recrystallized cornea and interior calcite of the eye lenses (specimen 2.6P, SE image). C: A highly polished telephinid eye lens that contains micro-crystalline dolomite crystals and micro-pitting (specimen T_178_sp10, BSE image). D-E: EBSD images of an asaphid specimen in thin section showing crystallographic continuity within the lenses (D) and the preservation of radial trabeculae structures (E) (specimen A_178_sp1). Image D is an inverse pole figure map overlain on an image quality map, and image E is an orientation tolerance map overlain on an image quality map. F: Lenses that are completely recrystallized, top and base of lenses marked by white lines, the basal boundary is unclear due to

crystal overgrowths (specimen 1.1B_sp1, BSE image, thin section). G: EBSD inverse pole figure map (overlain on an image quality map) of recrystallized lenses, with calcite crystals overlapping the lens boundaries (specimen 1.2C_sp2, thin section). H: Eye specimen with varying luminescence of the lenses under CL; L = luminescent; NL = non-luminescent, SL = slightly luminescent (specimen HV_sp43, thin section). Scale bars 500 μm (A, H), 50 μm (B-G).

In those specimens classified as poorly preserved, the eye lenses exhibit major alteration and lack pristine microstructures such as trabeculae. The microstructural evidence for extensive alteration of calcite lenses is as follows: 1. indistinct lens boundaries where the calcite crystals cross the lens-sediment boundary, form sub-crystals, or exhibit calcite twinning; 2. extensive pitting, resulting from the loss of small crystals and the presence of micropores, indicating that the lenses are recrystallized (Figure 3F); 3. a wide range of crystallographic orientations within a lens, indicating large-scale recrystallization (Fig. 3G); 4. The lens calcite is luminescent (Figure 3H). Minor alteration of lens calcite is evident by variable or partial luminescence due to trace amount variations in Mn and Fe, which can be detected by SEM and electron microprobe analysis. Under CL, recrystallization can be recognised by zoning in the lens calcite crystals and a luminescence intensity that is high, and similar to calcite spar cements in the host rock. Lenses that are more significantly altered can contain diagenetic quartz, dolomite and pyrite crystals.

Micro-dolomite crystals are present within the lenses of nine eye specimens (some well-preserved and others poorly preserved), and are associated with a pervasive microporosity/micro-pitting (Figure 3C). In some specimens, celestine can be recognised in BSE images as small white (i.e., high mean atomic number) crystals. Micro-crystalline dolomite is absent from the eyes of the Horn Valley Siltstone Formation trilobites, which are the most highly altered, and also does not occur in the cuticle. Micro-crystalline dolomite of a similar crystal size, celestine and a microporous texture are also features of the eyes of phacopine trilobites (Lee et al., 2007, 2012).

Trilobite eyes from the Valhallfonna Formation were analyzed using the electron microprobe to test for geochemical variation. The range in trace elements for calcite eyes is 0.6 - 1.9 wt% $MgCO_3$, 0 - 0.9 wt% $FeCO_3$ and 0 - 0.5 wt% $MnCO_3$. Trilobite eyes that are luminescent (and classified as poorly preserved) have slightly elevated Mn concentrations relative to non-luminescent lenses. There is no significant difference in the composition of eye calcite compared to that of the associated trilobite cuticle, or carbonate in the host sedimentary deposit (micrite and calcite spar) (Appendix B). Eyes containing micro-crystalline dolomite do not exhibit higher levels of Mg compared to those without micro-crystalline dolomite.

Specimens of trilobite cuticle from the Valhallfonna Formation were examined (Appendix A and B). Eight of the 44 studied had an internal structure comprising two layers of aligned crystals (Figure 4A), although most specimens lacked any internal structure. The cuticle is composed of prismatic, interlocking calcite micro-spar, with a consistent crystal size (Figure 4B), and no evidence of an outer prismatic layer of coarser crystals. EBSD of cuticle associated with trilobite eyes showed that in all specimens the cuticle crystals are randomly oriented. Some specimens have small euhedral pyrite crystals on the margins of the cuticle fragment, or in the interior. Most specimens are non-luminescent, but others exhibit partial or bright orange luminescence. Cuticle from six samples was analyzed by electron microprobe, with a maximum concentration of 2.3 wt% $MgCO_3$, 0.2 wt% $FeCO_3$, 0.4 wt% $MnCO_3$ and 0.6 wt% $SrCO_3$. In comparison to the trilobite eyes, the cuticles contain relatively pure calcite with low trace element concentrations. The size of the calcite crystals within the cuticle was measured from SEM images (Figure 4C), and average size does not correlate with the size of the cuticle fragment examined or its chemical composition (Appendix A and B).

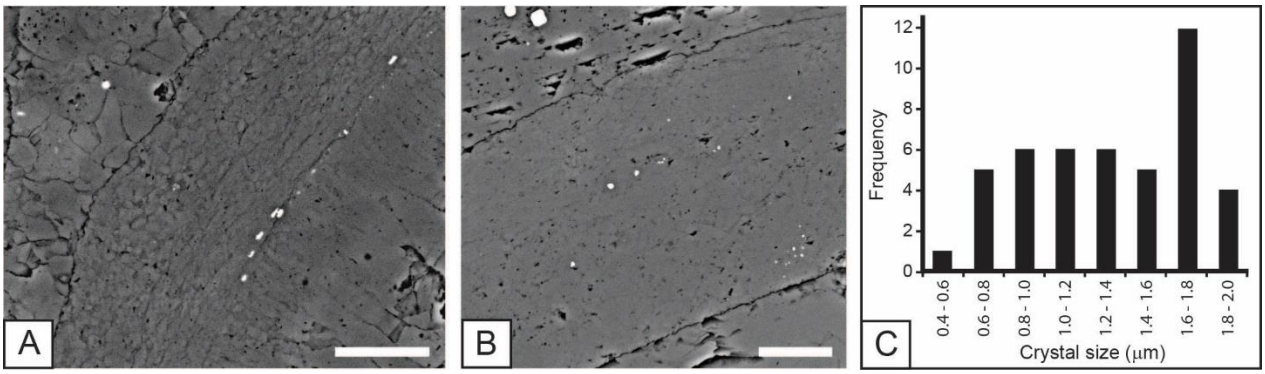

Figure 4. Trilobite cuticle preservation. A-B: Polished thin section, BSE images. A: *Carolinites sibiricus* cuticle with an internal structure of aligned crystals on the inner region (to the right), and larger crystals on the outer region. The crystal size is relatively large and small pyrite crystals are present on the internal margin of the specimen (sample 1.1B). B: *Carolinites genacinaca* cuticle with no internal structure and a relatively small crystal size (sample 1.2C_N_TS2). C: Plot of cuticle crystal size frequency. Scale bars for A and B are 25 μm.

In summary, specimens with the best-preserved eyes are from the Emanuel Formation, with nine out of thirteen eyes classified as well-preserved. Apart from one eye, all from the Valhallfonna Formation are poorly preserved. All eyes from the Horn Valley Siltstone are poorly preserved. Trilobite cuticles from the Valhallfonna Formation have variable microstructure, and EBSD shows that they lack any consistent crystallographic orientation. Well-preserved eyes have an integral preservation of lens calcite with a single crystallographic orientation and a composition of low-Mg calcite. In contrast, poorly preserved specimens exhibit multiple smaller crystals within a lens, unclear lens boundaries, luminescence, and varied chemical composition.

4.2 Stable Isotope Data

In total, 50 trilobite eyes were analyzed for isotope composition from the three formations, and where possible, the preservation state of each specimen was assessed prior to isotope analyses using the protocols described above (Appendix C). There is no difference in $\delta^{13}C$ and $\delta^{18}O$ between trilobite eye calcite extracted by a hand-held dental drill and that extracted by micro-mill (conventional isotope analysis

methods), or from clumped isotope analysis. For $\delta^{18}O$, there is a significant difference between conventional isotope analysis (Figure 5) and SIMS isotope results (Figure 6).

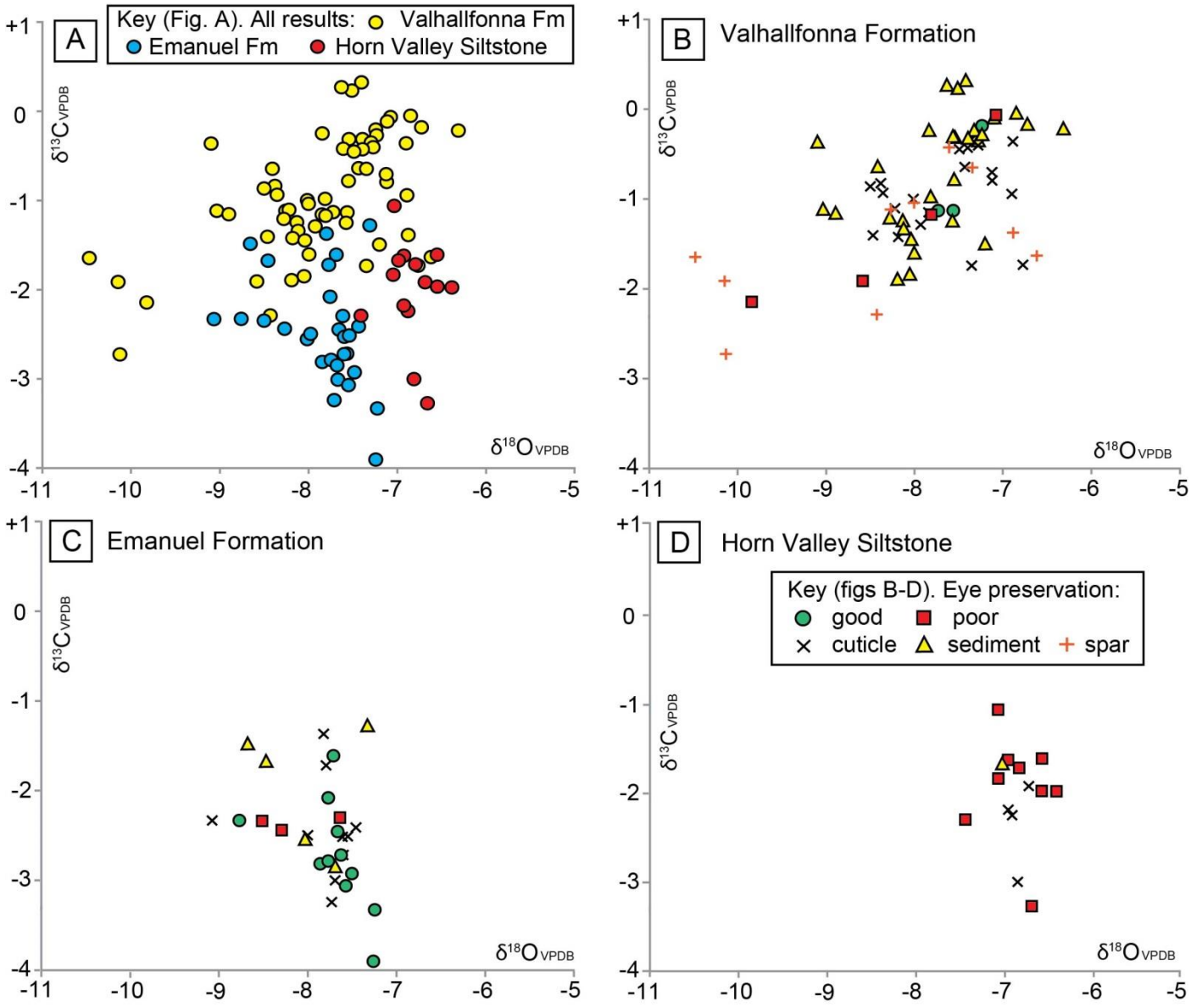

Figure 5. Dental drill and micro-mill $\delta^{18}O$ and $\delta^{13}C$ conventional isotope results for the three formations studied. A: All results (trilobite eye, cuticle and host rock), plotted by individual formation. B: Results from the Valhallfonna Formation, including trilobite eyes and other material. C: Results from the Emanuel Formation. D: Results from the Horn Valley Siltstone, note that all the eyes from this formation are interpreted to be poorly preserved. The key to symbols for graphs B-D is illustrated within D.

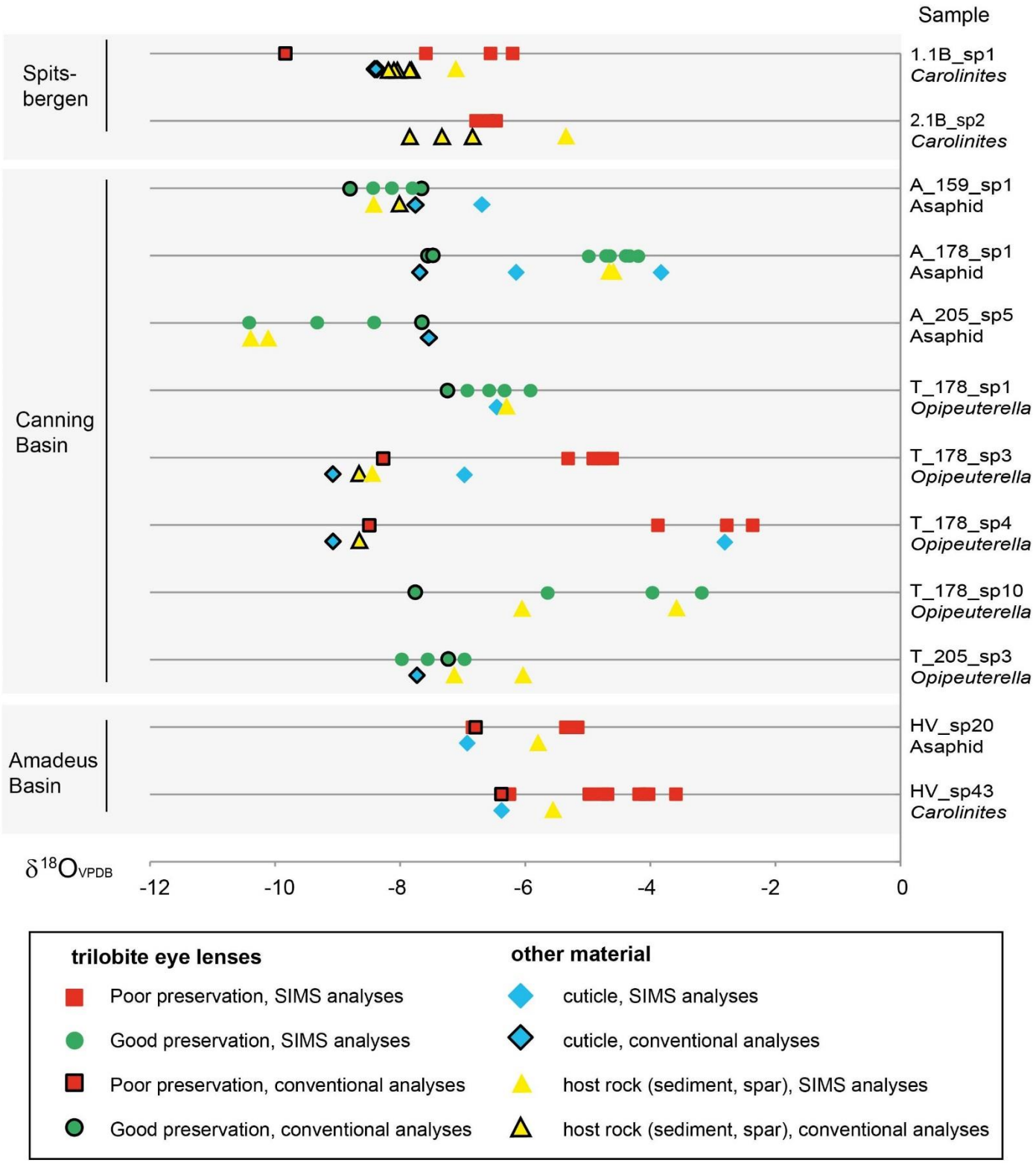

Figure 6. $\delta^{18}O$ results from SIMS analysis plotted against conventional isotope results, for individual specimens, including results from trilobite eye calcite, cuticle and rock.

4.2.1 Conventional Isotope Results

The total ranges in isotope composition for trilobite eyes (independent of preservation state), cuticle, and host rock (sediment and spar) analyzed are $\delta^{18}O$ –6.3‰ to –10.5‰ and $\delta^{13}C$ +0.3‰ to –3.9‰. Each formation plots in a different, but overlapping, $\delta^{13}C$ and $\delta^{18}O$ field (Figure 5A), and within each formation the trilobite eye isotope values are within the range of the results from the trilobite cuticle and host rock (Figure 5B-D).

With regards to the Valhallfonna Formation, the combined isotope results from all material (trilobite eyes, cuticle and host rock) show a low covariance between $\delta^{13}C$ and $\delta^{18}O$ ($R^2 = 0.28$) with values ranging from $\delta^{13}C$ +0.3‰ to –2.7‰ and $\delta^{18}O$ –6.3‰ to –10.5‰. This result is different from the other formations, which lack any covariance between $\delta^{13}C$ and $\delta^{18}O$ ($R^2 = 0.13$ Emanuel Formation; $R^2 = 0.01$ Horn Valley Siltstone). Well-preserved trilobite eyes yield $\delta^{18}O$ that are on average higher than those of poorly preserved eyes, ranging from $\delta^{18}O$ –7.2‰ to –7.7‰, although there is some overlap (Figure 5B). There is no significant difference in isotope composition between *Carolinites* species, stratigraphic units, or between the cuticle of *Carolinites* and olenid trilobites (Appendix C). The $\delta^{13}C$ or $\delta^{18}O$ variation between cuticle specimens that were identified as having relatively small or large calcite crystals is also negligible.

Results for all materials from the Emanuel Formation range from $\delta^{18}O$ of –7.3‰ to –9.1‰ and $\delta^{13}C$ of –1.3‰ to –3.9‰. Well-preserved trilobite eyes have a similar range in $\delta^{13}C$ and $\delta^{18}O$ to that of poorly preserved eyes (Figure 5C). There is no significant difference in isotope composition between the planktonic *Opipeuterella* sp. and benthic asaphid trilobites, or between different samples (Appendix C). It is possible that the outlier well-preserved eye result of $\delta^{18}O$ –8.8‰ is lower than the other well-preserved eye results due to the presence of diagenetically altered matrix material underlying the calcite lenses. Post-sampling photographs after the micro-mill had powdered the lenses do not indicate that this is the case, however the

imprecision of the micro-mill technique compared to intra-lens sampling by SIMS means that all micro-mill samples must be considered to be subject to some sediment contamination.

Results for all materials from the Horn Valley Siltstone have a fairly narrow range of $\delta^{18}O$ –6.4‰ to –7.4‰ and a broader range of $\delta^{13}C$ –1.1‰ to –3.3‰. All eyes examined were poorly preserved and there is no difference in isotope composition between the planktonic *Carolinites genacinaca* and benthic asaphid trilobites, or between different samples (Appendix C).

The isotope composition of lenses containing micro-crystalline dolomite does not differ from those composed purely of calcite. All samples were analyzed as calcite and it is uncertain whether dolomite crystals even contributed to the signal due to the small quantity of dolomite present (<1%). The presence of dolomite does not correspond to the preservation state of the eyes (Table 1).

Four larger well-preserved specimens were analyzed to test the average isotope variation across the eye. For each specimen, two sub-samples were taken for isotope analysis using the micro-mill or dental drill. Two of the specimens had a consistent composition in both sub-samples, while the other two showed a different composition, with a variability of up to circa 1‰ in $\delta^{18}O$ and $\delta^{13}C$ (Appendix C).

Twenty-one specimens with cuticle material attached to the eye (such as the librigena or glabella) were analyzed to compare the composition of the cuticle and adjacent eye lenses. In well-preserved specimens from the Valhallfonna Formation, the cuticle is similar in composition to that of the eyes (with a maximum difference in $\delta^{18}O$ of 0.6‰) while in poorly preserved specimens the difference is greater (increasing to $\delta^{18}O$ 2.4‰) (Appendix C). In the Emanuel Formation, the composition of the cuticle is similar to that of the eyes (with a difference in $\delta^{18}O$ of 0.8‰) for asaphids and *Opipeuterella* sp., with no significant difference between poorly preserved and well-preserved specimens (Appendix C). However, the difference in $\delta^{18}O$ between eyes and cuticle from the Horn Valley Siltstone, which contains only poorly preserved specimens, is less than 0.2‰.

4.2.2 SIMS Oxygen Isotope Results

SIMS analysis of individual lenses across trilobite eyes in thin section reveals a wide range in $\delta^{18}O$, from –2.4‰ to –10.4‰ (Table 2). The range can dramatically vary even within specimens identified as well-preserved, and is often different from the conventional isotope analysis results of the same specimen extracted using the dental drill or micro-mill (Fig. 6). For most of the 12 specimens analyzed, the lens composition is within the general range of $\delta^{18}O$ as that of cuticle and host rock. However, many of the SIMS results for trilobite eyes, cuticle and host rock yield $\delta^{18}O$ values that are substantially more positive than the conventional isotope analysis results.

Specimens identified as well-preserved and poorly preserved have SIMS $\delta^{18}O$ results within the same range, and there is no correlation with specimens that have micro-crystalline dolomite within the lenses. The average $\delta^{18}O$, and the range of $\delta^{18}O$ within a single eye, does not correlate with the state of preservation of the eyes. There is no difference between the results from telephinids and asaphid specimens from the same formation, even in well-preserved eyes.

Multiple lenses of individual specimens were analyzed using SIMS, giving an intra-eye $\delta^{18}O$ range, with the greatest range seen within a single eye specimen of 2.7‰ and the lowest range of 0.3‰. Eight specimens have a relatively high $\delta^{18}O$ range (1‰ or greater), while four have a low range in values (less than 1‰) (Figure 6).

The SIMS and conventional isotope analysis results for individual specimens show some variations. All trilobite cuticle analyses of specimens from the two methods show a high disparity (with $\delta^{18}O$ difference greater than 1‰) (Figure 6). Eleven trilobite eye specimens were assessed by SIMS and conventional isotope analysis, and of these, six specimens have a high disparity between the SIMS and conventional methods, while five specimens had similar results ($\delta^{18}O$ <1‰ difference). There is no apparent link between the analysis conditions (beam intensity, chamber pressure, measurement error, run order) and those trilobite

eye samples with a large range in $\delta^{18}O$ (see Supplementary Information). In general, $\delta^{18}O$ results obtained by SIMS are more positive (by as much as 6‰) in comparison to those obtained by conventional isotope analysis.

4.2.3. Clumped Isotope Results

Of the 12 samples examined for their Δ_{47} compositions, the cuticle and limestone analyzed from Västergötland had markedly low Δ_{47} values of $\Delta_{47CDES25}$ = +0.383 and +0.396‰, respectively [reported against the absolute Carbon Dioxide Equilibrated Scale - hereafter CDES - reference frame described by Dennis et al. (2011) and referring to CO_2 extracted by phosphoric acid digestion at 25°C]. These values correspond to very high "apparent equilibrium temperature" (over 200°C, see Appendix D) representing the "blocking temperature" with respect to diffusional resetting of the calcite clumped isotope thermometer (e.g., Passey and Henkes, 2012; Bonifacie et al., 2013).

In contrast, the range in $\Delta_{47CDES25}$ values for the three other basins investigated in this study is much higher (with $\Delta_{47CDES25}$ from 0.581 to 0.610‰ for Spitsbergen, 0.608 to 0.623‰ for the Canning Basin and 0.606 to 0.608‰ for the Amadeus Basin; Appendix D). These Δ_{47} values correspond to temperature ranges of 55-68°C (average 63°C) for the Valhallfonna Formation, 50-56°C (average 52°C) for the Emanuel Formation and 56-57°C for the Horn Valley Siltstone Formation, respectively (Figure 7). These temperature estimates were calculated from the Δ_{47}-T universal calibration published by Bonifacie et al. (2016) defined on all (Ca, Mg, Fe)CO_3 carbonates. Only small differences in $\delta^{18}O$ are observed between cuticle and limestone (up to 0.45 ‰: Appendix D) and there is no difference in temperatures (derived from Δ_{47} data) between those of the host rock and cuticle from the same sample. These results indicate that all fossil calcite materials analyzed have experienced (and imprinted a Δ_{47} signature characteristic of) higher temperatures than those at which they originally precipitated in Ordovician seawater.

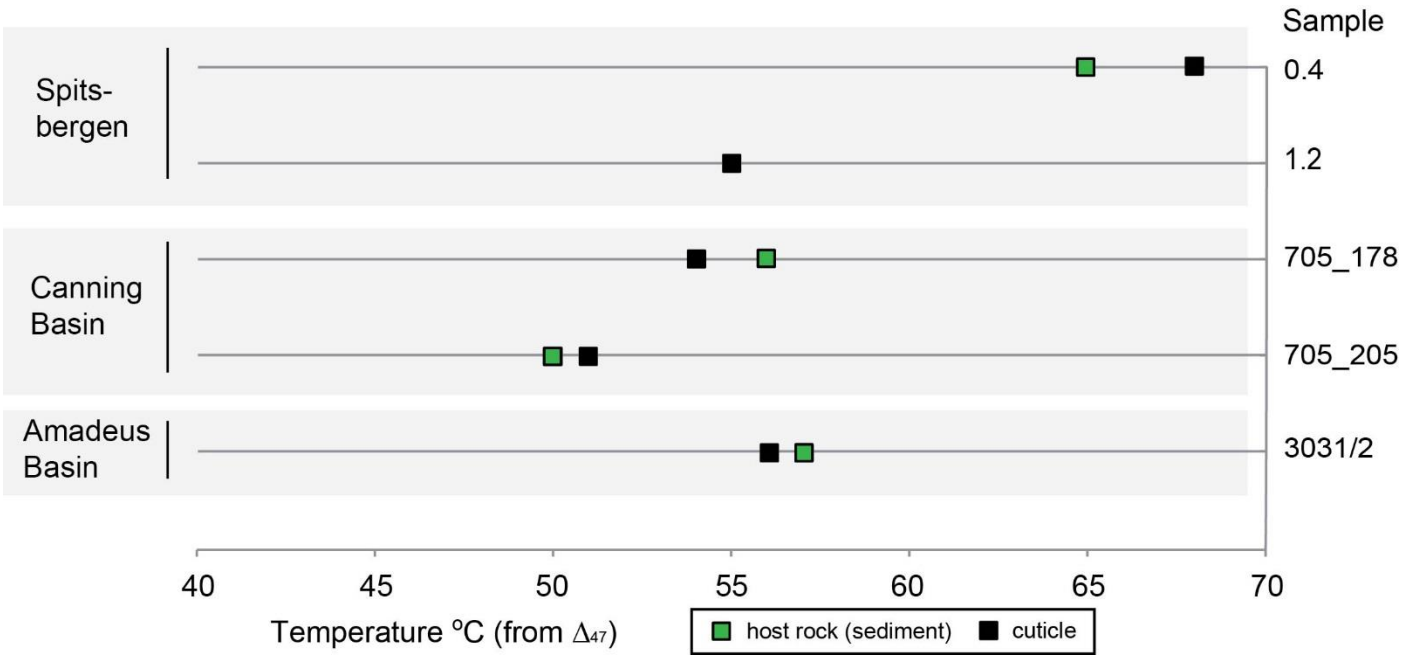

Figure 7. Clumped isotope temperature estimates from Δ_{47} for the three main formations studied. For further details including conventional isotope $\delta^{18}O$ and $\delta^{13}C$ results, Δ_{47} values and reconstructed water $\delta^{18}O_{water}$, see Appendix D.

The $\delta^{18}O_{water}$ from which the calcite in these three formations was precipitated was calculated using the temperature estimated from Δ_{47} and the $\delta^{18}O$ of the carbonate, and referenced to published Ordovician $\delta^{18}O_{VSMOW}$ estimates. They correspond to $\delta^{18}O_{water}$ of –0.4 to +1.0‰ (average 0.2‰) for the Valhallfonna Formation, –1.6 to –0.2‰ (average –0.9‰) for the Emanuel Formation and 0.0 to +0.6‰ (average +0.3‰) for the Horn Valley Siltstone (Appendix D). Because the Δ_{47} signatures found here do not represent those acquired over original carbonate crystallisation from seawater, the calculated $\delta^{18}O_{water}$ of the mineralizing fluid cannot be interpreted in terms of the original seawater $\delta^{18}O$, but rather likely reflects the properties of diagenetic fluids. However because the $\delta^{18}O_{water}$ results are fairly comparable to that estimated for Ordovician seawater (–1‰ $\delta^{18}O_{VSMOW}$: Trotter et al., 2008) it is probable that diagenesis may have occurred due to the flow of seawater through the rocks during burial, down to a maximum depth of two kilometres.

5. Discussion

The eye preservation assessment using a combined methodology (SEM, CL, EBSD and electron microprobe) indicates a range in degrees of alteration. The preservation of the trabeculae has been described as an indicator of good eye preservation (Schoenemann and Clarkson, 2011), but it has also been noted that trabeculae can be preserved in diagenetically altered specimens (Torney et al., 2014). The cornea (outermost layer of the trilobite eye) is likely to have been a transparent sheet *in vivo* (Clarkson et al., 2006), and its present micro-crystalline state indicates that it was recrystallized during diagenesis. The loss of *in vivo* microstructures from trilobite cuticle indicates that the majority have been recrystallized: the outer prismatic layer (Dalingwater, 1973; Dalingwater et al., 1991) is absent, the presence of pyrite within the cuticle is consistent with diagenetic alteration (Wilmot, 1990), as is the homogeneous microstructure of the calcite (Budil and Hörbinger, 2007). As the cuticle is thought to mineralize in an organic mesh-like framework, similar to that of an ostracod carapace (Teigler and Towe, 1975), the lack of correspondence between crystal size and size of the exoskeleton may indicate diagenesis. Large cuticle crystals may be expected to have incorporated trace-elements or have a different isotope composition to microcrystalline cuticle calcite. Moreover, the crystallographic orientation of the cuticle crystals (observed to be random under EBSD) has changed, with crystal c-axis perpendicular to the cuticle surface (Teigler and Towe, 1975).

In terms of the visual protocols used to assess preservation, the most useful method was EBSD analysis, due to the crystallographic orientation information it shows. SEM microstructural observations were also valuable and identified porosity and micro-crystals (Table 1). While CL generally corresponded to other indicators, with luminescent lenses showing an elevated trace-element profile and evidence for recrystallization, lenses that were recrystallized were sometimes non-luminescent. Thus, CL is the least reliable technique, however it does generate visual data that can be used as a starting point for more detailed preservation analysis via other techniques.

The SIMS results differ significantly from the corresponding conventional isotope analysis results in over half the trilobite eye specimens analyzed. This discrepancy may be due to presence of a fine-scale mixture of primary and secondary calcite within the lenses. In addition, little is known about the composition of

trilobite cuticle, or vital effects, in comparison to brachiopods where studies on modern specimens can be used to determine $\delta^{18}O$ paleotemperature equations (Brand et al., 2013). However, it must also be considered that the inconsistency between analytical datasets could reflect a systematic analytical error in the SIMS data in this study. Previous work has found differences in the trace element content (Mg/Ca, Sr/Ca and Mn/Ca ratios) of marine bivalves analyzed using conventional bulk dissolution and SIMS. These differences have been interpreted as reflecting variable shell organic content, crystal structures and small inter-crystalline heterogeneities in trace element concentrations (Freitas et al., 2009). It is therefore possible that the presence of organic matter within trilobite eyes, sub-crystal boundaries, or pitted surfaces could have affected our SIMS data. However, the cross-comparison of the SIMS results with the micro-crystalline characteristics of each specimen (Table 1) does not reveal a correspondence between the presence of micro-crystalline features (porosity, crystal zoning, micro-dolomite) and wide ranging or positive $\delta^{18}O$ values. The size of the ion beam used for the SIMS analysis (15 μm) may have resulted in the crossing of crystal boundaries, although most of the spots sampled the centre region of the eye lens and were verified by photographs. It is more likely that the results represent genuine intra-eye variation rather than contamination from the host rock. Further detailed work is needed to attempt to correct the SIMS data for the variables of inter-crystalline heterogeneities. The SIMS analysis has revealed large intra-eye variations of lens geochemistry that would otherwise remain undetected. Despite the limitations of the method, for example micro-scale pitting and sub-crystal boundaries that may cause analytical error, SIMS is still a useful tool for assessing diagenesis.

The range of isotope compositions within a single eye specimen (as revealed by both SIMS and conventional isotope analysis) indicates cryptic recrystallization. This means that recrystallization has likely occurred in specimens that were identified as well-preserved using the SEM, CL, EBSD and electron microprobe protocols outlined above. Ten out of the sixteen specimens examined had ranges in $\delta^{18}O$ of greater than 1‰ within the same eye. If, as seems reasonable, all the lenses in an eye were biomineralized (or indeed recrystallized) at the same time, in the same conditions, then they should have the same isotope

composition. For each formation, there is no significant difference in $\delta^{18}O$ or $\delta^{13}C$ between trilobite eye calcite or cuticle and the host rock. In addition: 1. all trilobite cuticle examined is interpreted as diagenetically altered, with a complete loss of crystallographic structure, indicating recrystallization was pervasive; 2. calcitic spar within the host rock, typically resulting from diagenetic growth, is within the same isotope range as the trilobite eye and cuticle results (Fig. 5B); and 3. the counterintuitive finding that pelagic trilobite species, which lived in relatively warm waters near the sea surface, have the same $\delta^{18}O$ as benthic species, indicates that all $\delta^{18}O$ has been reset. Therefore, most, if not all, of the material analyzed is interpreted to have been diagenetically altered, despite our original assessment of good preservation using microstructural criteria. In terms of eye preservation, there is little geochemical difference between eyes identified as well-preserved or poorly preserved, both in terms of conventional isotope analysis and SIMS results. In addition, the degree of recrystallization (complete or partial) has no significant correspondence with the isotope results.

Detailed SIMS analysis shows a large range in $\delta^{18}O$ values within a single eye specimen, even those that on microstructural criteria are well-preserved. Our preservation assessment can therefore be criticised for not identifying subtle preservation features. For example, the presence of trabeculae and lens crystallographic continuity as identified by EBSD mapping was interpreted to indicate well-preserved eyes, but the boundaries of the trabeculae were not examined in detail using TEM as they were by Torney et al. (2014). Micro-crystalline dolomite was observed in well-preserved and poorly preserved specimens, and further analysis using TEM is needed to further understand the origin of this mineral. Despite these limitations, the present study has made the most extensive preservation assessment of any trilobite material prior to isotope analysis.

The presence of micro-crystalline dolomite within the holochroal eyes examined here may indicate an original high-Mg calcite composition (as interpreted for the eyes of phacopine trilobites by Lee et al., 2012), with high-Mg calcite being diagenetically altered to low-Mg calcite. The presence of micro-crystalline

dolomite in both poorly- and well-preserved eyes, supports this interpretation. The absence of micro-crystalline dolomite in the Horn Valley Siltstone samples may be due to their more extensive diagenetic alteration. However, the lenses containing micro-crystalline dolomite do not have an elevated Mg content, as recorded in phacopine eyes, of up to 6 mol% $MgCO_3$ (Lee et al., 2007, 2012). This could be due to the diagenetic loss of magnesium over time. However, the sporadic occurrence of microcrystalline-dolomite - it is not present in all eyes identified as well-preserved - means that at present we cannot conclude that the holochroal lenses were originally composed of high-Mg calcite. An alternative explanation might be that the dolomite grew during diagenetic alteration and micro-recrystallisation of low-Mg calcite. Further detailed investigation of the micro-crystalline dolomite at the nanometre scale is needed to determine an original high-Mg calcite composition of the lenses.

The host rock and fossil material from each of the three basins have a distinctive range in $\delta^{13}C$ and $\delta^{18}O$ values, which may reflect their different diagenetic histories. The Δ_{47} data reveal a minimum temperature of trilobite cuticle (re)crystallisation of 50ºC, which is well in excess of the threshold for most organisms living in the surface layers of the modern oceans (Brock, 1985) and must be interpreted as resulting from the diagenetic alteration of the original cuticle. The Västergötland cuticle clumped isotope results are at the extreme temperature end (200°C), where the original Δ_{47} values (i.e. the original ^{13}C–^{18}O bonding distribution acquired over crystallisation) have been reset due to closed-system solid-state diffusion alteration. This conclusion is consistent with independent Västergötland CAI values of 6 to 7, indicative of peak temperatures exceeding 300ºC resulting from heating by Permian igneous intrusions (Bergström, 1980). In contrast, the Australian and Spitsbergen samples have lower temperatures calculated from the Δ_{47} (from 50-68ºC; Figure 7), which reflect early recrystallization temperatures.

The thermal history of the sedimentary formations can be linked to the fidelity of eye preservation. The Emanuel Formation was subject to the lowest burial temperatures (maximum temperatures of 70-80ºC: Nicoll et al., 1993) and its sample set contains the best-preserved trilobite eyes. The Valhallfonna Formation

was subject to a slightly higher burial temperature (up to 90°C: Bergström, 1980) and its sample set contains just one well-preserved specimen. While the Horn Valley Siltstone experienced a much higher burial temperature (up to 140°C: Gibson et al., 2007) and yielded no well-preserved specimens.

It could be argued that the conventional $\delta^{18}O$ and $\delta^{13}C$ results for the trilobite cuticle, eyes and host rock reflect original compositions and were not affected by partial recrystallization and only the Δ_{47} composition changed. Indeed, solid-state re-ordering can alter the C-O bonds within a shell while retaining original shell microstructures and trace-element concentrations (Henkes et al., 2014). Experimental studies on brachiopod shells by Henkes et al. (2014) have shown that solid-state reordering can start to reset the original C-O bonds (and thus Δ_{47} compositions) of calcite if it experienced temperatures above 100°C for more than hundreds of millions of years. Stolper and Eiler (2015) argue that reordering can start to occur at temperatures of 75°C, and becomes more significant over 120°C. To explore this possibility further, the thermal history of each basin must be examined in terms of the duration spent at higher temperatures during burial. The detailed burial history of Ny Friesland, Spitsbergen has not yet been reconstructed. The Canning Basin experienced temperatures of 70-80°C for approximately 200 Myr in the Mesozoic, but only underwent a brief higher temperature interval of ~100°C (Arne et al., 1989) or <90°C (Wallace et al., 2002) in the early Carboniferous, making solid state diffusion unlikely. The Stairway Sandstone, which overlies the Horn Valley Siltstone in the Amadeus Basin, experienced burial temperatures of over 100°C in the Permian-Triassic (for approximately 80 million years), and Cretaceous (for approximately 110 million years) (Gibson et al., 2007). It is possible that solid-state diffusion may have affected the specimens from the Horn Valley Siltsone, although the time that the rocks experienced temperatures over 100°C is fairly short. Overall, low-temperature recrystallization, over solid-state diffusion, is the most likely mechanism responsible for altering the trilobite eyes and cuticle.

Figure 8 shows trilobite $\delta^{18}O$ data from the present study plotted against published geochemical data from trilobite cuticle and brachiopods through the Ordovician. There are no published data available for Lower

Ordovician trilobites, but those from the Middle and Upper Ordovician range from $\delta^{18}O$ of –3‰ to –7‰ (McAlister and Brand, 1989; Brand, 2004; Finnegan et al., 2011), which is within the range of that recorded in the present study. Ordovician-Silurian studies comparing brachiopods and trilobites found them to have a similar $\delta^{18}O$ to each other (McAlister and Brand, 1998; Wilmot and Fallick, 1989). While Finnegan et al. (2011) found Upper Ordovician trilobites to have a similar $\delta^{18}O$ composition to that of contemporaneous brachiopods and corals. Of all the published trilobite isotope studies, that by Finnegan et al. (2011) is the only one where the preservation of the trilobite cuticle has been examined via trace element and microstructural studies, prior to isotope analysis.

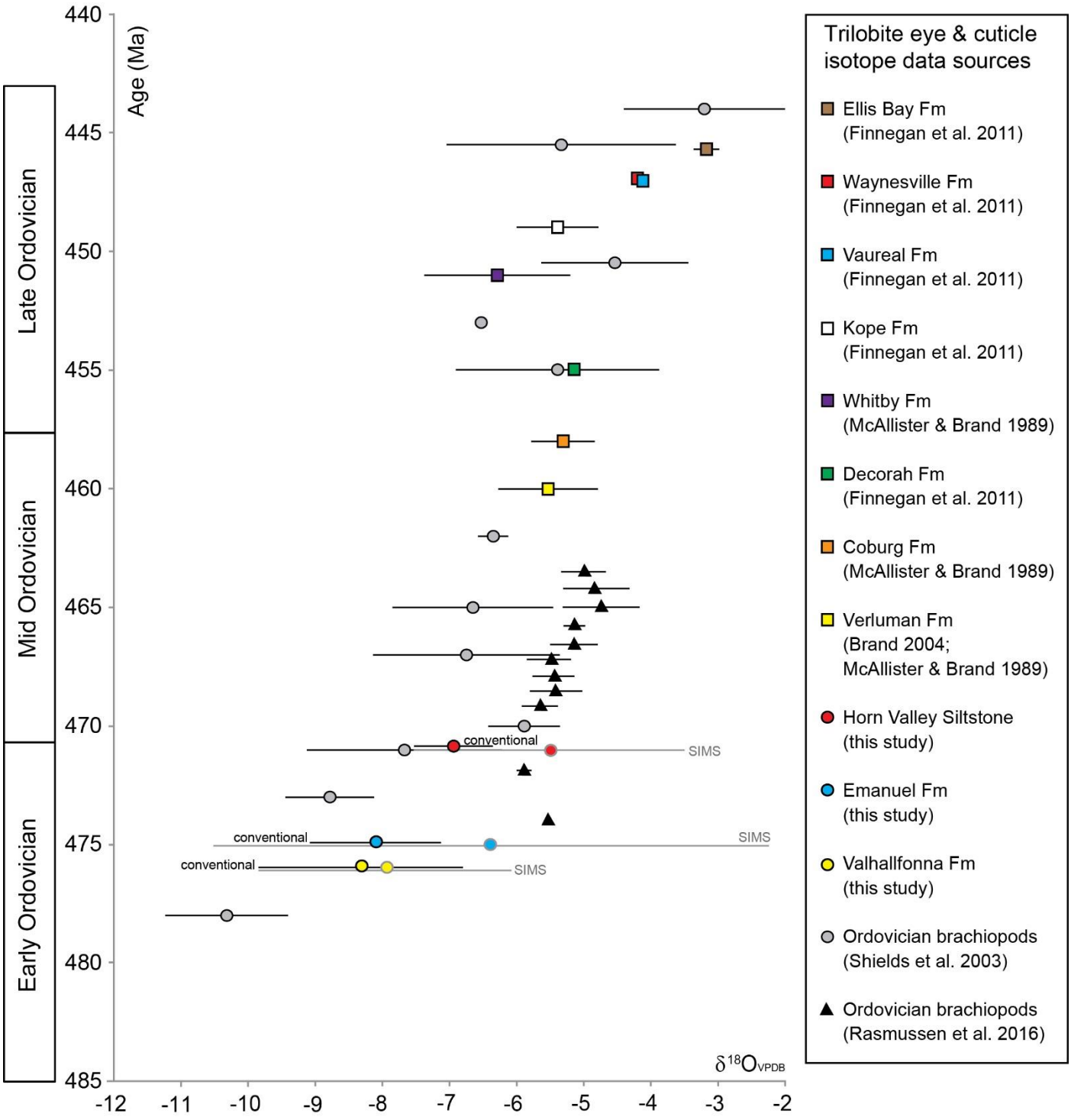

Figure 8. Trilobite eye and cuticle data from this study (conventional isotope analysis and SIMS), plotted with trilobite cuticle data from the literature, and brachiopod data (Shields et al., 2003; Rasmussen et al., 2016). Grey and black bars are isotope ranges, with the mean isotopic value indicated by the symbol in the centre.

The $\delta^{18}O$ data from trilobites in the present study are within the range of contemporaneous brachiopods, or more positive (Figure 8). The exceptions are new data from Baltica which have higher $\delta^{18}O$ values (Rasmussen et al., 2016). Given our results, this raises questions about the possibility of brachiopod calcite recrystallization from some earlier studies. Brachiopod specimens from the Lower to Middle Ordovician that were analyzed by conventional isotope techniques were assessed for preservation using trace element geochemistry and SEM and CL characterization (Veizer et al., 1999; Shields et al., 2003), but not by EBSD or SIMS. Significant cryptic diagenesis may have altered the isotope composition of these specimens: in general it is thought that only the secondary layer of the brachiopod shell is reliably unaltered and the preservation state of this layer can vary between taxonomic groups (Garbelli et al., 2012); In addition, SIMS analysis of brachiopods reveals that within certain groups, the secondary layer is only precipitated in isotope equilibrium with seawater towards the innermost part of the shell (Cusack et al., 2012). This fact implies that isotope studies where the entire secondary layer was analyzed (for example Shields et al., 2003) may reflect non-equilibrium fractionation. This is variable between brachiopod groups, for example in spiriferid brachiopods the prismatic tertiary layer is more resistant to diagenesis than the secondary layer (Grossman et al., 1993). Even in samples that have experienced low burial temperatures, recrystallisation can occur: in a study of Silurian brachiopods, Cummins et al. (2014) argued that elevated clumped isotope temperatures (up to 56^{o}C) found in samples with CAI = 1 were likely resulting from diagenetic alteration due to recrystallization. This result cautions the use of apparently pristine biogenic specimens to interpret ancient paleotemperatures, without prior carbonate clumped isotope analysis. Due to the effects of sold-state reordering of clumped isotopes, which may not alter $\delta^{13}C$ and $\delta^{18}O$ values, analysis using the range of methods utilised in this study (SIMS, CL, SEM and EBSD) should be combined to jointly assess fossil preservation and isotope geochemistry.

Brachiopod data have been used to suggest that the $\delta^{18}O$ of Ordovician seawater was lower than at the present-day (–3‰ $\delta^{18}O_{VSMOW}$) in order to account for a reasonable paleotemperature calculation for the most negative $\delta^{18}O$ results (Veizer et al., 1999; Shields et al., 2003). Modelling of long-term seawater

geochemical composition estimates of Ordovician $\delta^{18}O_{VSMOW}$ at approximately –6‰ (Jaffrés et al., 2007), and a revised calibration of the brachiopod data gives a value of –5‰ $\delta^{18}O_{VSMOW}$ for the Early Ordovician at 475 Ma (Veizer and Prokoph, 2015). However, Trotter et al. (2008) used a value of –1‰ to interpret the temperature of formation of Ordovician conodont apatite, giving similar ocean temperatures for the Early Ordovician to that interpreted from the brachiopod data. The Ordovician brachiopod calcite, trilobite calcite and conodont apatite (Trotter et al., 2008; Veizer and Prokoph, 2015) isotope data show an increase in carbonate or phosphate $\delta^{18}O$ values over the Ordovician, which indicates either cooling oceans, changing seawater chemistry, or increasing diagenetic imprints at higher temperature with time. Conodont apatite has been demonstrated to be well-preserved (Wheeley et al., 2012) and is therefore useful as a paleotemperature proxy in the Paleozoic (Joachimski and Buggisch 2002). The results of Trotter et al. (2008) indicate that conodont apatite may be a much more reliable proxy than brachiopod calcite, as it yields more reasonable ocean paleotemperature calculations. How do the trilobite results influence this debate? The diagenetic alteration of trilobites demonstrated here reveals that the most negative $\delta^{18}O$ values in the Early to Middle Ordovician (those less than $\delta^{18}O$ –7‰) are probably the result of diagenesis rather than a distinctive seawater composition. Results of the present study therefore bring into question the fidelity of some Early-Middle Ordovician brachiopod records and call for a re-appraisal. The new positive $\delta^{18}O$ brachiopod data by Rasmussen et al. (2016) for the Early Ordovician highlight the need for a review of all brachiopod data from this time. As no EBSD or SIMS work has been undertaken on Lower to Middle Ordovician trilobite or brachiopod specimens analyzed for their isotope composition prior to this study, the possibility remains that significant cryptic diagenesis may have altered these specimens. We therefore caution the interpretation of isotope results without rigorous preservation assessment and advise that SIMS analysis should be added to the tool-box of preservation studies.

6. Conclusions

- The holochroal eyes of species of the pelagic trilobite genera *Carolinites* and *Opipeuterella* from the Floian (Lower Ordovician) Valhallfonna Formation, Spitsbergen, and the Floian-Dapingian (Lower-

Middle Ordovician) Emanuel and Horn Valley Siltstone formations of Australia were examined to assess their preservation state.

- The use of trilobite eyes for vision places strict constraints on the *in vivo* microstructure of their constituent calcite lenses, and as such is a unique means of guiding our preservation assessment.
- The microstructure and chemical composition of the eyes was assessed using SEM, CL, EBSD and electron microprobe. The Valhallfonna and Emanuel formations contain the best-preserved specimens, based on these assessment protocols. Well-preserved eyes are composed of low-Mg calcite, are non-luminescent, have clear crystallographic boundaries and retain their original optical structures such as trabeculae.
- Trilobite cuticle is composed of low-Mg calcite, but the wide range of crystal size within the cuticle, random crystal orientation and lack of original structures indicates that all specimens have been recrystallized.
- The $\delta^{18}O$ and $\delta^{13}C$ results show a different range for each formation. However, intra-eye isotope analyses using SIMS reveals a large range in $\delta^{18}O$ in some specimens, of up to 2.7‰. There is also no systematic isotope difference between rock, cuticle, eyes and diagenetic cements, or between benthic and pelagic trilobite eyes or cuticle.
- A sub-set of trilobite cuticles from the three formations was analyzed with carbonate clumped isotope thermometry, generating a temperature range of 50-68^{o}C and so indicating low-temperature diagenetic alteration of the trilobite calcite.
- Despite rigorous preservation assessment protocols, the SIMS and Δ_{47} data both show that all trilobite eye and cuticle specimens analyzed here have, at least in part, been diagenetically altered, including those that were interpreted to be well-preserved using microstructural criteria. The presence of sparse micro-crystalline dolomite within some eye specimens hints at cryptic recrystallization processes, although the impact of the presence of dolomite on the isotope results remains unclear.

- Despite clear evidence for alteration, $\delta^{18}O$ obtained in the present study are similar to those that have been previously used to infer Ordovician paleoceanographic conditions.
- We suggest that standard preservation assessment protocols may be insufficient for Paleozoic carbonates because of the difficulty in elucidating cryptic recrystallization that has taken place at low temperatures. Extensive microstructural analysis of Ordovician biogenic carbonates using EBSD in conjunction with SIMS and carbonate clumped isotope analysis is recommended before stable isotope signatures are used for paleoclimate or paleoenvironmental interpretation.

Acknowledgements

Geoscience Australia is thanked for the loan of trilobite specimens from the Emanuel Formation and Horn Valley Siltstone. Thanks also go to Claire Torney for invaluable discussions on *Carolinites* eye structure and preservation; Seth Finnegan (UC – Berkeley) for pilot clumped isotope investigations; Diederik Depla and Henk Vrielinck (Ghent University) for use of micro-saw facilities; Philippe Recourt (CNRS, Univ. Lille 1) for SEM photography; Claire Rollion-Bard, Michel Champenois and Denis Mangin (CRPG, CNRS, Nancy) for help with SIMS analyses. The Research Foundation – Flanders (FWO) is acknowledged for funding of isotope analyses (research grant 1.5.079.08); CNRS-INSU is acknowledged for funding of SIMS analyses (action SYSTER). The University of Lille 1 and the Research Foundation – Flanders (FWO) are thanked for funding the postdoctoral fellowships of CEB and TRAV respectively, during which most of this research was carried out. We would like to thank two anonymous reviewers for their thorough and helpful reviews of this manuscript. This is a contribution to IGCP 591: 'The Early to Middle Paleozoic Revolution', and IGCP 653: 'The onset of the Great Ordovician Biodiversification Event'. The data to support the conclusions in this text can be found in Table 1 and in appendices A-D of the Supplementary Information.

References

Amberg, C., T. Collart, W. Salenbien, L. M. Egger, A. Munnecke, A. T. Nielsen, C. Monnet, Ø. Hammer, and T. R. A. Vandenbroucke (2016), The nature of Ordovician Limestone-mudstone alternations in the

Oslo-Asker area (Norway): witnesses of primary glacio-eustasy or diagenetic rhythms? *Scientific Reports, 6,* doi: 10.1038/srep18787.

Arne, D. C., P. F. Green, I. R. Duddy, A. J. W. Gleadow, I. B. Lambert, and J. F. Lovering (1989), Regional thermal history of the Lennard shelf, Canning Basin, from apatite fission track analysis: Implications for the formation of Pb-Zn ore deposits. *Australian Journal of Earth Sciences: An International Geoscience Journal of the Geological Society of Australia, 36,* 495-513.

Bergström, S. M. (1980), Conodonts as paleotemperature tools in Ordovician rocks of the Caledonides and adjacent areas in Scandinavia and the British Isles. *Geologiska Föreningen i Stockholm Förhandlingar, 102,* 377-392.

Bickert, T., J. Pätzold, C. Samtleben, and A. Munnecke (1997), Paleoenvironmental changes in the Silurian indicated by stable isotopes in brachiopod shells from Gotland, Sweden. *Geochimica et Cosmochimica Acta, 61,* 2717-2730.

Bonifacie, M., D. Calmels, and J. Eiler (2013), Clumped isotope thermometry of marbles as an idicator of the closure temperatures of calcite and dolomite with respect to solid-state reordering of C–O bonds. *Goldschmidt abstract 2013*.

Bonifacie, M., D. Calmels, J. M. Eiler, J. Horita, C. Chaduteau, C. Vasconcelos, P. Agrinier, A. Katz, B. H. Passey, J. M. Ferry and J. – J. Bourrand. (2016), Calibration of the dolomite clumped isotope thermometer from 25 to 350°C, and implications for a universal calibration for all (Ca, Mg, Fe)CO_3 carbonates. *Geochimica et Cosmochimica Acta,* doi: http://dx.doi.org/10.1016/j.gca.2016.11.028.

Brand, U. (2004), Carbon, oxygen and strontium isotopes in Paleozoic carbonate components: an evaluation of original seawater-chemistry proxies. *Chemical Geology, 204,* 23-44.

Brand, E., K. Azmy, M. A. Bitner, A. Logan, M. Zuschin, R. Came, and E. Ruggiero (2013), Oxygen isotopes and $MgCO_3$ in brachiopod calcite and a new paleotemperature equation. *Chemical Geology, 359*, 23-51.

Brock, T. D. (1985), Life at high temperatures. *Science, 230*, 132-138.

Budil, P., and F. Hörbinger (2007), Exoskeletal structures and ultrastructures in Lower Devonian dalmanitid trilobites of the Prague Basin (Czech Republic). *Bulletin of Geosciences, Czech Geological Society, Prague, 82*, 27-36.

Clarkson, E., R. Levi-Setti, and G. Horváth (2006), The eyes of trilobites: The oldest preserved visual system. *Arthropod structure and development, 35*, 247-259.

Coplen, T. B. (1988), Normalisation of oxygen and hydrogen isotope data. *Chemical Geology, 72*, 293-297.

Cummins, R. C., S. Finnegan, D. A. Fike, J. M. Eiler, and W. W. Fischer (2014), Carbonate clumped isotope constraints on Silurian ocean temperature and seawater $\delta^{18}O$. *Geochimica et Cosmochimica Acta, 140*, 241-258.

Cusack, M., A. Pérez-Huerta, and Edinburgh Ion Microprobe Facility (2012), Brachiopods recording seawater temperature – A matter of class or maturation? *Chemical Geology, 334*, 139-143.

Dalingwater, J. E. (1973), Trilobite cuticle microstructure and composition. *Paleontology, 16*, 827-839.

Dalingwater, J. E., S. J. Hutchinson, H. Mutvei, and D. J. Siveter (1991), Cuticular ultrastructure of the trilobite *Ellipsocephalus Polytomus* from the Middle Cambrian of Öland, Sweden. *Palaeontology, 34*, 205-217.

Dennis, K. J., H. P. Affek, B. H. Passey, D. P. Schrag, and J. M. Eiler (2011), Defining an absolute reference frame for 'clumped' isotope studies of CO_2. *Geochimica et Cosmochimica Acta, 75*, 7117-7131.

Finnegan, S., K. Bergmann, J. M. Eiler, D. S. Jones, D. A. Fike, I. Eisenman, N. C. Hughes, A. K. Tripati, and W. W. Fischer (2011), The magnitude and duration of Late Ordovician-Early Silurian glaciation. *Science, 331,* 903-906.

Fortey, R. A. (1975), The Ordovician trilobites of Spitsbergen. 11. Asaphidae, Nileidae, Raphiophoridae and Telephinidae of the Valhallfonna Formation. *Norsk Polarinstitutt Skrifter, 162,* 1-207.

Fortey, R. A., and C. R. Barnes (1977), Early Ordovician conodont and trilobite communities of Spitsbergen: influence on biogeography. *Alcheringa, 1,* 297-309.

Fortey, R. A., and D. L. Bruton (2013), Lower Ordovician Trilobites of the Kirtonryggen Formation, Spitsbergen. *Fossils and Strata, 59,* 1-116.

Fortey, R. A., and D. L. Bruton (1973), Cambrian-Ordovician rocks adjacent to Hinlopenstretet, North Ny Friesland, Spitsbergen. *Geological Society of America Bulletin, 84,* 2227-2242.

Freitas, P. S., L. J. Clarke, H. Kennedy, and C. A. Richardson (2009), Ion microprobe assessment of the heterogeneity of Mg/Ca, Sr/Ca and Mn/Ca ratios in *Pecten maximus* and *Mytilus edulis* (bivalvia) shell calcite precipitated at constant temperature. *Biogeosciences Discuss., 6,* 1267-1316.

Friedman, I., and J. R. O'Neil (1977), Compilation of stable isotope fractionation factors of geochemical interest. *Professional Paper US Geological Survey* 440.

Garbelli, C., L. Angiolini, F. Jadoul, and U. Brand (2012), Micromorphology and differential preservation of Upper Permian brachiopod low-Mg calcite. *Chemical Geology, 298-299,* 1-10.

Gibson, H. J., I. R. Duddy, G. J. Ambrose, and T. R. Marshall (2007), Regional perspectives on new and reviewed thermal history data from central Australian basins. In: Munson T.J. and Ambrose G.J. 2007. *Proceedings of the Central Australian Basins Symposium, Alice Springs, 16-18th August, 2005.* Northern Territory Geological Survey. Special Publication 2. pp11-36.

Ghosh, P., J. Adkins, H. Affek, B. Balta, W. F. Guo, E. A. Schauble, D. Schrag, and J. M. Eiler (2006), ^{13}C-^{18}O bonds in carbonate minerals: A new kind of paleothermometer. *Geochimica et Cosmochimica Acta, 70*, 1439-1456.

Grossman, E.L., Mii, H.S. and T.E. Yancey, (1993), Stable isotopes in Late Pennsylvanian brachiopods from the United States: Implications for Carboniferous paleoceanography. *Geological Society of America Bulletin, 105*, 1284-1296.

Henkes, G. A., B. H. Passey, E. L. Grossman, B. J. Shenton, A. Perez-Huerta, and T. E. Yancey (2014), Temperature limits for preservation of primary calcite clumped isotope paleotemperatures. *Geochimica et Cosmochimica Acta, 139*, 362–382.

Henkes, G.A., B. H. Passey, A. D. Wanamaker, E. L. Grossman, W. G. Ambrose, and M. L. Carroll (2013), Carbonate clumped isotope compositions of modern marine mollusk and brachiopod shells. *Geochimica et Cosmochimica Acta, 106*, 307-325.

Huntington, K. W., J. M. Eiler, H. P. Affek, W. Guo, M. Bonifacie, L. Y. Yeung, N. Thiagarajan, B. Passey, A. Tripati, M. Daëron, and R. Came (2009), Methods and limitations of 'clumped' CO_2 isotope ($\Delta 47$) analysis by gas-source isotope ratio mass spectrometry. *Journal of Mass Spectrometry, 44*, 1318-1329.

Jaffrés, J. B. D., G. A. Shields, and K. Wallmann (2007), The oxygen isotopic evolution of seawater: A critical review of a long-standing controversy and an improved geological water cycle model for the past 3.4 billion years. *Earth-Science Reviews, 83,* 83-122.

Joachimski, M.M. and W. Buggisch (2002), Conodont apatite δ18O signatures indicate climatic cooling as a trigger of the Late Devonian mass extinction. *Geology*, *30,* 711-714.

Laurie, J. R. (2006), Ordovician trilobites from the Horn Valley Siltstone and basal Stairway Sandstone, Amadeus Basin, Northern Territory. *Memoirs of the Association of Australian Paleontologists, 32*, 287-345.

Laurie, J. R., and J. H. Shergold (1996), Early Ordovician trilobite taxonomy and biostratigraphy of the Emanuel Formation, Canning Basin, Western Australia, Parts 1 and 2. *Paleontographica Abt. A., 240*, 65-144.

Lee, M. R., C. Torney, and A. W. Owen (2007), Magnesium-rich intralensar structures in schizochroal trilobite eyes. *Palaeontology, 50*, 1031-1037.

Lee, M. R., C. Torney, and A. W. Owen (2012), Biomineralisation in the Paleozoic oceans: Evidence for simultaneous crystallisation of high and low magnesium calcite by phacopine trilobites. *Chemical Geology, 314-317*, 33-34.

McAlister, J. E., and U. Brand (1989), Geochemistry of some Ordovician and Devonian trilobite cuticles from North America. *Chemical Geology, 78*, 51-63.

McCormick, T., and R. A. Fortey (1998), Independent testing of a paleobiological hypothesis: the optical design of two Ordovician pelagic trilobites reveals their relative paleobathymetry. *Paleobiology, 24*, 235-253.

McCormick, T., and R. A. Fortey (1999), The most widely distributed trilobite species: Ordovician *Carolinites genacinaca. Journal of Paleontology, 73*, 202-218.

McRoberts, C. A., T. A. Hegna, J. J. Burke, M. L. Stice, S. K. Mize, and M. J. Martin (2013), Original spotted patterns on Middle Devonian phacopid trilobites from western and central New York. *Geology, 41*, 607-610.

Nicoll, R. S., Laurie, J. R. and M. T. Roche (1993), Revised stratigraphy of the Ordovician (Late Tremadoc-Arenig) Prices Creek Group and Devonian Poulton Formation, Lennard Shelf, Canning Basin, Western Australia. *AGSO Journal of Australian Geology and Geophysics, 14*, 65-76.

Passey, B. H., and G. A. Henkes (2012), Carbonate clumped isotope bond reordering and geospeedometry. *Earth and Planetary Science Letters, 351*, 223–236.

Pohl, A., Y. Donnadieu, G. Le Hir, J. - F. Buoncristiani, and E. Vennin (2014), Effect of the Ordovician paleogeography on the (in)stability of the climate. *Climate of the Past, 10*, 2053-2066.

Pohl, A., Y. Donnadieu, G. Le Hir, J.-B. Ladant, C. Dumas, J. Alvarez-Solas and T. R. A. Vandenbroucke (2016), Glacial onset predated Late Ordovician climate cooling. *Paleoceanography, 31*, 800–821.

Pruss, S. B., S. Finnegan, W. W. Fischer, and A. H. Knoll (2010), Carbonates in skeleton-poor seas: new insights from Cambrian and Ordovician strata of Laurentia. *Palaios, 25*, 73-84.

Rasmussen, C. M. Ø, C. V. Ullmann, K. G. Jakobsen, A. Lindskog, J. Hansen, T. Hansen, M. E. Eriksson, A. Dronov, R. Frei, C. Korte, and A. T. Nielsen (2016), Onset of main Phanerozoic marine radiation sparked by emerging Mid Ordovician icehouse. *Scientific Reports*, 6, 18884, doi: 10.1038/srep18884.

Rollion-Bard, C., D. Mangin, and M. Champenois (2007), Development and application of oxygen and carbon isotopic measurements of biogenic carbonates by Ion Microprobe. *Geostandards and Geoanalytical Research, 31*, 39-50.

Schoenemann, B., and E. N. K. Clarkson (2011), Light guide lenses in trilobites? *Earth and Environmental Science Transactions of the Royal Society of Edinburgh*, *102*, 17–23.

Shields, G. A., G. A. F. Carden, J. Veizer, T. Meidla, J. - Y. Ronga, and R. - Y. Li (2003), Sr, C, and O isotope geochemistry of Ordovician brachiopods: A major isotopic event around the Middle-Late Ordovician transition, *Geochimica et Cosmochimica Acta*, *67*, 2005–2025.

Stolper, D.A., and J.M. Eiler (2015), The kinetics of solid-state isotope-exchange reactions for clumped isotopes: A study of inorganic calcites and apatites from natural and experimental samples. *American Journal of Science*, *315*, 363-411.

Teigler, D. J., and K. N. Towe, (1975), Microstructure and composition of trilobite cuticles. *Fossils and Strata*, 4, 137–149.

Torney, C., M. R. Lee, and A. W. Owen (2014), Microscructure and growth of the lenses of schizochroal trilobite eyes. *Palaeontology, 57*, 783-799.

Trotter, J. A., I. S. Williams, C. R. Barnes, C. Lecuyer, and R. S. Nicoll (2008), Did cooling oceans trigger Ordovician biodiversification? Evidence from conodont thermometry, *Science, 321*, 550-554.

Vandenbroucke, T. R. A., H. Armstrong, M. Williams, J. Zalasiewicz, and K. Sabbe (2009), Ground-truthing Late Ordovician climate models using the paleobiogeography of graptolites. *Paleoceanography, 24*, PA4202.

Veizer, J., D. Ala, K. Azmy, P. Bruckschen, D. Buhl, F. Bruhn, G. A. F. Carden, A. Diener, S. Ebneth, Y. Godderis, T. Jasper, C. Korte, F. Pawellek, O. G. Podlaha, and H. Strauss. (1999), $^{87}Sr/^{86}Sr$, $\delta^{13}C$ and $\delta^{18}O$ evolution of Phanerozoic seawater. *Chemical Geology*, *161*, 59-88.

Veizer, J. and A. Prokoph, (2015), Temperatures and oxygen isotopic composition of Phanerozoic oceans. *Earth-Science Reviews*, *146*, 92-104.

Wadleigh, M.A. and J. Veizer, (1992), $^{18}O^{16}O$ and $^{13}C^{12}C$ in lower Paleozoic articulate brachiopods: Implications for the isotopic composition of seawater. *Geochimica et Cosmochimica Acta*, *56*, 431-443.

Wallace, M.W., Middleton, H.A., Johns, B. and Marshallsea, S., Hydrocarbons and Mississippi Valley-type sulfides in the Devonian reef complexes of the eastern Lennard Shelf, Canning Basin, Western Australia. In: Keep M. and Moss S.J. (2002), *The sedimentary basins of Western Australia 3. Proceedings of the West Australian basins Symposium*. Perth, Petroleum Exploration Society of Australia. pp. 795-816.

Wilmot, N. V. (1990), Primary and diagenetic microstructures in trilobite exoskeletons. *Historical Biology, 4*, 51-65.

Wilmot, N. V., and A. E. Fallick, (1989), Original mineralogy of trilobite exoskeletons. *Palaeontology, 32*, 297-304.

Wheeley J. R., M. P. Smith, and I. Boomer (2012). Oxygen isotope variability in conodonts: implications for reconstructing Paleozoic palaeoclimates and paleoceanography. *Journal of the Geological Society, London, 169*, 239-250.

Supplementary Information and Appendices

Supplementary Material (extended version)

Valhallfonna Formation

Trilobites were sampled from the Valhallfonna Formation, Floian (Arenigian) of Ny Friesland, Spitsbergen, during the Cambridge University and Oslo Paleontological Museum expeditions of 1967 and 1971 (Fortey, 1975). Samples containing abundant telephinid trilobites with intact eye lenses were selected for the present study from the Nileid and Olenidsletta biofacies from the Olenidsletta and Profilbekken members. The sedimentary deposits of the Valhallfonna Formation are composed of calcareous shales, sparitic limestone and dark bedded limestone (Fortey and Bruton, 1973). Both the Olenidsletta and Profilbekken members contain telephinid trilobites, along with a high diversity of other trilobite groups including olenids and asaphids (Fortey, 1975). The depositional environment is interpreted to be deeper than that of the underlying Kirtonryggen Formation, but still that of a marine shelf setting (Fortey and Barnes, 1977; Fortey and Bruton, 2013). The burial history of Ny Friesland is thought to be shallow, with Conodont Alteration Index (CAI) values of 1 suggesting maximum temperatures of 90ºC (Bergström, 1980).

Forty-three trilobite eyes were examined from eleven samples. Eleven eyes were assessed for preservation in thin section, of which eight were analyzed for their carbon and oxygen stable isotope compositions. Trilobite eyes and cuticle examined were from the telephinid *Carolinites* (*C. angustagena, C. genacinaca, C. nevadensis* and *C. sibiricus*), along with cuticle (but no eyes) from benthic olenids (species indeterminate). Clumped isotope Δ_{47} analyses were undertaken on rock sediment and cuticle (indeterminate species) from two samples.

Emanuel Formation

Trilobites were studied from the Emanuel Formation, Floian (Bendigonian) of the Canning Basin, Western Australia (Laurie and Shergold, 1996). Samples were selected that contained abundant telephinid and asaphid trilobites with intact eye lenses. The Emanuel Formation is composed of calcareous shales, siltstones and limestones, some of which are nodular (Laurie and Shergold, 1996). The burial history for the Canning Basin has been determined by Apatite Fission Track Analysis (AFTA) to indicate temperatures of ~100ºC during the Late Devonian/Early Carboniferous (Arne et al., 1989).

Fifty-one trilobite eyes were examined from five samples, from the type section of the Emanuel Formation (Laurie and Shergold, 1996). Thirteen eyes were assessed for preservation in thin section and were analyzed for their isotopic composition. Trilobite eyes examined were from the telephinid *Opipeuterella* sp. and benthic asaphids (species indeterminate). Δ_{47} analyses were undertaken on asaphid cuticle and rock sediment from two samples.

Horn Valley Siltstone

Trilobites were studied from the Horn Valley Siltstone, Floian to Dapingian (Bendigonian to Yapeenian) of the Amadeus Basin, Northern Territory, Australia (Laurie, 2006). Samples were selected that contain abundant telephinid and asaphid trilobites with intact eye lenses. The Horn Valley Siltstone is composed of calcareous siltstone, with minor sandstone, limestone and silty dolostone, containing abundant fossils including trilobites of the orders Asaphida, Proetida, Phacopida and Agnostida (Laurie, 2006). Based on conodont and trilobite biostratigraphy, the Horn Valley Siltstone may be correlatable with the upper part of the Emanuel Formation and the overlying Gap Creek Formation from the Canning Basin (Laurie, 2006). The burial history for the Amadeus Basin has been determined by AFTA and organic maturity data that indicate maximum burial during the Pennsylvanian (Late Carboniferous), with Ordovician strata subjected to maximum temperatures of 140ºC (Gibson et al., 2007).

Over 100 trilobite eyes were examined from three samples collected from a field section at Mt Olifent (Laurie, 2006, fig. 6). Nine eyes were assessed for preservation in thin section and were analyzed for their

isotopic composition. Trilobite eyes examined were from the telephinid *Carolinites genacinaca* and benthic asaphids (species indeterminate). Δ_{47} analyses were undertaken on asaphid cuticle and rock sediment from one sample.

Västergötland

Two test samples of *Telephina* cuticle and rock sediment were analyzed for Δ_{47} from the Upper Member of the Dalby Limestone, Sandbian (Late Ordovician), from Ludibunduskalksten, Västergötland, Sweden. The Västergötland rocks have been heated by local Permian intrusions, giving CAI values of 6 to 7 and temperatures of over 300^{o}C (Bergström, 1980). Eyes were not examined from this section, but thin sections of the *Telephina* cuticle were produced in order to assess the material prior to clumped isotope analysis.

Supplementary Methods (extended version)

Preservation assessment protocol

In total, 198 trilobite eyes were examined under reflected light using a binocular microscope, which allowed an initial assessment of eye lens integrity and preservation. SEM analysis of these specimens allowed the examination of the micro-structure of the lens interior and the cornea. 34 large specimens representing a range of preservation states, were selected for thin section analysis based on the eye size (greater than 1.8 mm length).

Prior to thin sectioning, eyes were halved with a micro-saw, and one half set aside for isotope analyses. Thin sections were produced by hand polishing slices of trilobite eyes and mounting them in epoxy resin. Polished thin sections were examined under CL using a cold cathode optical system operated at an accelerating voltage of with a 15 kV and 380 nA µm beam current. Geochemical variation in eye specimens was quantified using a Cameca SX100 electron microprobe at the University of Lille, using a 15 kV

accelerating voltage, 15 nA current and 1µm beam diameter. A JEOL JXA-8600S electron microprobe was also used at the University of Leicester, using a 15 kV accelerating voltage, 30 nA current and 15 µm beam diameter. 20 second count times were used for measurement of characteristic peak intensities, with 10 seconds at each of the background positions selected on either side of the peak. Calcium, magnesium, manganese, iron and strontium compositions were analyzed, quantitative results were calibrated to standards used for carbonate analysis, with an analytical error of less than 0.1wt% for both instruments.

Trilobite eye specimens were imaged under high vacuum on a FEI Quanta 200 SEM at the University of Lille and a Hitachi S-3600N SEM at the University of Leicester, using Secondary Electron and Back Scattered Electron detectors. EBSD analysis of polished thin sections was undertaken at the University of Glasgow to examine lens crystallographic orientations (Torney et al., 2014). This was performed on a FEI Quanta 200F field emission environmental scanning electron microscope (FEG-ESEM), with an EDAX–TSL integrated ED–EBSD system running OIM version 5.2.1 software. Prior to EBSD work the thin sections were briefly polished with colloidal silica in order to enhance the quality of Kikuchi patterns, and were analyzed uncoated and at low vacuum. Here the EBSD results are expressed in three ways. Image quality maps represent the quality of the Kikuchi patterns, with those patterns containing well defined bands producing white/light grey pixels and the poor-quality patterns (for example from epoxy resin or points where two crystals overlap) giving black/dark grey pixels. The inverse pole figure maps represent the crystallographic orientation of calcite crystals using a colour scale, whereby a different colour corresponds to a different orientation. This colour scale is presented and explained in Torney et al. (2014). Orientation tolerance maps use a colour scale to show how orientations differ from a reference point in the map. These maps are used to reveal subtle orientation contrasts, as for example may occur between the constituent trabeculae of a lens. Blue and green colours indicate a small orientation difference whereas yellow and red indicates a larger difference.

Isotope Analyses

202 isotope analyses were run on trilobite eyes, cuticle and host rock from all three formations (Appendix C). Where possible, the preservation state of the trilobite eyes examined for isotopes was assessed prior to isotope analysis using the protocols described above. 25 eye specimens were analyzed for isotopes from the Valhallfonna Formation (of which 16 specimens had been assessed for preservation), 16 from the Emanuel Formation (15 of which had been assessed for preservation) and 9 from the Horn Valley Siltstone (all assessed for preservation).

$\delta^{18}O$, $\delta^{13}C$ and Δ_{47} analyses were performed using three analytical methods; 1) conventional isotope $\delta^{18}O$ and $\delta^{13}C$ analyses of about 0.5 mg carbonate powder, with lens/cuticle extraction using both a hand-held dental drill and automated micro-mill; 2) SIMS $\delta^{18}O$ analyses of a 15 μm diameter area of a thin section; 3) and clumped isotope analyses (Δ_{47}) measured together with $\delta^{18}O$ and $\delta^{13}C$ of about 8 mg of carbonate powder.

Conventional $\delta^{18}O$ and $\delta^{13}C$ analyses. Carbonate powders extracted by hand-held dentist-drill were analyzed using the conventional isotope analysis method at the British Geological Survey, UK and using a micro-mill automated New Wave Research MicroMill at the University of Erlangen, Germany. At NIGL carbonate powders of about 0.5 mg were reacted with 100% phosphoric acid at 90°C using a multiprep device attached to an IsoPrime dual inlet mass spectrometer. Reproducibility was checked by replicate analysis of laboratory standards (KCM) and is better than ± 0.05‰ (1σ). At Erlangen, carbonate powders were reacted with 100% phosphoric acid at 70°C using a Gasbench II connected to a ThermoFinnigan V Plus mass spectrometer. Reproducibility was checked by replicate analysis of international laboratory standards (SOL 1 and IAEA CO-9) and is better than ± 0.06‰ (1σ). At both institutions stable carbon and oxygen isotope values are reported in standard delta notation relative to the VPDB standard.

SIMS $\delta^{18}O$ analyses were undertaken at the Centre de Recherches Pétrographiques et Géochimiques (CRPG-CNRS) facility in Nancy, France. A CAMECA IMS 1270 ion microprobe (Rollion-Bard et al., 2007) was operated with a beam diameter of 15 μm, for 1 second counts. The $\delta^{18}O_{VSMOW}$ values were

converted to $\delta^{18}O$ using the Coplen (1988) equation: $\delta^{18}O_{PBD}$ Sample = (0.97002 x $\delta^{18}O_{VSMOW}$ sample) – 29.98. Reproducibility was checked by replicate analysis of laboratory standards (MEX and NBS calcite crystals), giving an average error of $\delta^{18}O_{VSMOW}$ ±0.3‰. The standards were analysed in between each trilobite sample data-point. Throughout the run of samples there was a gradual increase in beam intensity and the pressure in the chamber was subject to minor fluctuations. The beam was not re-tuned between each sample. Variations in the $\delta^{18}O_{VSMOW}$ results do not correspond to analytical error, beam intensity or chamber pressure variables. Matrix effects (such as sampling contamination by host rock) were mitigated by carefully selecting the lenses to analyse on thin section photographs, with the verification of the correct sampling points via post-sampling photographs.

Carbonate clumped isotope (Δ_{47}) analyses. The new Δ_{47} paleothermometer is particularly interesting for paleotemperature reconstruction because it is independent of the $\delta^{18}O$ of mineralizing fluids (Ghosh et al., 2006). It is based on the temperature-dependant preference of rare isotopes ^{13}C and ^{18}O to bond with each other within the mineral lattice at low temperatures. Because any Δ_{47} measurement comes with simultaneous determination of $\delta^{18}O$ and $\delta^{13}C$ of the analyzed carbonate, Δ_{47} thermometry provides independent estimates of the temperature of crystallisation (and/or recrystallization) and the $\delta^{18}O$ composition of the mineralizing fluid. However, when carbonates have been deeply buried and/or experienced high temperature conditions for extended periods of time, diagenetic alteration can also occur as a closed-system solid-state diffusive reordering of atoms within the mineral lattice, leading to lower Δ_{47} values and higher apparent equilibrium temperatures (e.g., Passey and Henkes, 2012; Bonifacie et al., 2013; Henkes et al., 2014; Stolper and Eiler, 2015). The original ^{13}C and ^{18}O distribution within the mineral lattice can be changed without affecting the $\delta^{18}O$ or $\delta^{13}C$ bulk isotopic composition of calcite, its trace metal content or microstructure. However, experimental studies investigating closed-system diffusive reordering suggest that temperature limits for the preservation of primary calcite clumped isotope paleotemperatures are relatively high (i.e. calcites

experiencing 100°C or lower for 10^6 to 10^8 year timescales should not be affected; Passey and Henkes, 2012; Henkes et al., 2014).

Carbonate clumped isotopes analyses were undertaken at the Institut de Physique du Globe de Paris (IPGP, Stable Isotope team). A detailed description of the IPGP setup is given in Bonifacie et al. (2016) and is briefly summarized here. For each analysis, about 8 mg of sample were digested for 20 minutes in 104% phosphoric acid at 90°C using a common acid bath connected to a manual vacuum line. During the digestion step, produced gases (CO_2 and H_2O) were continuously transferred to a liquid nitrogen (LN_2) trap hold at -196°C. After complete digestion (extraction yields of 100.2 ± 2.5%), incondensable gases were pumped away and the trapped CO_2 was then cryogenically purified from H_2O by passing through an ethanol-LN_2 trap (-115 to -130°C). Purified CO_2 was then allowed to pass through a 10 cm long U-trap (6 mm, ID), held at -28°C, packed with silver wool (to remove sulphur compounds) and 7-8 cm of Porapak-Q, 50-80 mesh (to remove volatile organic compounds and remaining traces of water). Clean CO_2 was then transferred to the mass spectrometer Thermo Scientific MAT 253 and analyzed for its Δ_{47}, $\delta^{18}O$ and $\delta^{13}C$ within 15 minutes after purification. The MAT 253 was operated in dual inlet mode and configured to measure simultaneously masses 44 through 49 of the purified CO_2 versus a reference gas (Oztech with $\delta^{18}O$ = -15.79‰ and $\delta^{13}C$= -3.63%). Each measurement consisted of 7 acquisitions of 10 cycles (integration time of 26 seconds for each cycle) for a total integration time of 1820 seconds per analysis at bellows pressure adjusted to get 16V on mass 44. Carbonate clumped isotope composition (Δ_{47}) is defined as the excess of mass 47 in the analyzed CO_2 relative to what it should be if ^{13}C and ^{18}O isotopes were randomly distributed between all CO_2 isotopologues. The Δ_{47CDES} data are here referenced to the absolute reference frame (or CDES for Carbon Dioxide Equilibrated Scale) of Dennis et al. (2011) using an empirical transfer function (ETF) we built with multiple analyses of at least three different CO_2 gases (with variable $\delta^{13}C$ and $\delta^{18}O$ values) that were brought to thermodynamic equilibrium at either 1000°C or 25°C. As our samples were digested at 90°C, an acid correction factor of 0.092‰ (as found by Henkes et al., 2013 and verified at IPGP) was added to the Δ_{47} results in order to report the data in a 25°C acid digestion frame (ie. $\Delta_{47CDES25}$) to follow common protocol.

Accuracy and external reproducibility on Δ_{47} measurements was evaluated by repeat analyses of three carbonate reference materials that were also analyzed in the inter-lab comparison study of Dennis et al. (2011): NBS-19 (n=2), $\Delta_{47CDES25}$=0.386 ± 0.003‰ (mean±1σ, standard deviation); IPGP-Carrara (n=19), Δ_{47CDES}=0.406±0.012‰; GCAZ-01b (n=15), $\Delta_{47CDES25}$=0.718±0.013‰. The $\Delta_{47CDES25}$ values reported here for those three carbonate reference materials are indistinguishable from those obtained in previous studies (e.g., Dennis et al., 2011; Henkes et al., 2013) and from the longer term averages found at IPGP. The $\delta^{13}C$ and $\delta^{18}O$ values were normalized to the international standards NBS-19 ($\delta^{13}C$=1.95‰, $\delta^{18}O$= -2.20‰) and IAEA-CO-1 ($\delta^{13}C$=2.49‰, $\delta^{18}O$=-2.40‰).

The Δ_{47CDES} data were converted into temperatures using the universal composite Δ_{47}–T calibration defined by carbonates with growth temperatures ranging from -1°C to 300°C and analysed in seven different laboratories generating Δ_{47} data after high-temperature digestion of carbonate minerals (Bonifacie et al., 2016). Although other relationships between Δ_{47} and temperature have been published (e.g. Ghosh et al., 2006; Henkes et al., 2013), we preferred to apply this recent calibration to estimate temperatures out of our Δ_{47} data because this calibration covers the range of temperatures investigated here (avoiding propagation of errors when extrapolating out of the calibrated temperature ranges) and, most importantly, allows to standardize the temperature estimates out of different laboratories running high-temperature digestion of carbonates. Note, however, that applying other experimental Δ_{47}-T calibration relationships to our data, returns minimum crystallization temperatures that remain high, ranging for instance from 45°C (Ghosh et al., 2006) to 61°C (Henkes et al., 2013) – all well above the threshold for most life living in the surface layers of the oceans (Brock, 1985).

$\delta^{18}O_{VSMOW}$ of the water from which the calcite precipitated was calculated using the temperature estimated out of Δ_{47CDES} data, the $\delta^{18}O$ of the carbonate as well as the experimentally determined temperature dependence of the oxygen isotopes fractionation between carbonate and water from Friedman and O'Neil (1977).

1

2

Supplementary Tables

Appendix A. Trilobite cuticle preservation

Sample	Trilobite Species	CL	Probe	Internal Structure	Crystal Size	Fragment Width
0.1_N	unknown	n/a	-	none	2.0	65
		n/a	-	none	1.7	60
		n/a	-	none	1.3	115
		n/a	-	2 layers, crystals larger in outer	1.3	80
		n/a	-	none	1.7	48
		n/a	-	none	0.7	150
		n/a	-	none	2.0	250
		n/a	-	none	0.7	125
0.4	unknown	NL	Y	none	0.8	230
		NL	-	none	1.0	40
		n/a	-	none	1.3	220
1.1B	*Carolinites sibiricus*	NL	-	aligned crystals	0.7	75
		NL	-	none	0.9	75
		NL	-	crystal alignment on inner region	1.1	45
1.2C_N_TS1	*Carolinites genacinaca*	NL	Y	none	0.8	190
		NL	Y	2 layers, crystals larger in outer	0.9	92
1.2C_N_TS2	*Carolinites genacinaca*	n/a	-	none	1.7	90
1.3_N_TS1	*Carolinites genacinaca*	n/a	-	none	2.0	70
		n/a	-	none	2.0	51
1.3_N_TS2	*Carolinites genacinaca*	NL	Y	none	1.7	63
1.3G		n/a	-	surface only visible	1.7	n/a
1.4A_N	*Carolinites sibiricus*	NL	-	none	1.4	56
		NL	-	2 layers, crystals larger in outer	1.1	80
		n/a	-	none	1.7	120
		n/a	-	2 layers, crystals larger in outer	1.7	108
1.4B_N_TS1	*Carolinites sibiricus*	n/a	-	none	0.8	150
		n/a	-	none	0.8	130
1.4B_N_TS2	*Carolinites sibiricus*	n/a	-	none	1.0	80
2.1A	*Carolinites genacinaca*	n/a	-	surface only visible	1.3	n/a
2.1B	*Carolinites genacinaca*	SL	-	none	1.1	60
2.2C	*Carolinites genacinaca*	n/a	Y	2 layers, crystals larger in outer	1.4	250
		n/a	-	none	1.4	120
2.3	*Carolinites genacinaca*	n/a	-	none	1.7	52
2.4	*Carolinites nevadensis*	SL	-	none	0.7	29
2.4I	*Carolinites nevadensis*	n/a	-	alignment of cuticle crystals in section	1.4	50
2.4J_N	*Carolinites nevadensis*	NL	-	none	1.3	118
2.4K_N	*Carolinites nevadensis*	NL	Y	none	1.7	45
2.4K	*Carolinites nevadensis*	n/a	-	surface only visible	1.7	40
2.4L_N	*Carolinites nevadensis*	NL	-	none	1.7	25
2.5	*Carolinites* sp.	n/a	-	none	1.7	80
		n/a	-	none	1.3	70
2.5E	*Carolinites* sp.	n/a	-	surface only visible	1.4	n/a
2.6	*Carolinites angustagena*	n/a	-	surface only visible	0.5	n/a
2.7_N	*Carolinites* sp.	L	-	none	1.0	33

Trilobite cuticle preservation assessment data table, for specimens from the Valhallfonna Formation. Crystal size and specimen width are measured in micrometers (μm). Abbreviations: CL = cathodoluminescence; L = luminescent; NL = non-luminescent, SL = slightly luminescent; n/a = not applicable because the specimen was not analyzed; Probe = if the specimen was analyzed on the electron microprobe (see Appendix 1), indicated with a Y for yes and a dash for no.

1 Appendix B. Electron microprobe results

Sample	Specimen	Material Analyzed	CL results	$CaCO_3$	$Mg\ CO_3$	$Fe\ CO_3$	$Mn\ CO_3$	$Sr\ CO_3$
0.4		trilobite cuticle indet.	NL	98.2	1.0	0.0	0.2	0.6
		trilobite cuticle indet.	NL	98.4	1.3	0.0	0.0	0.3
		trilobite cuticle indet.	NL	98.3	1.0	0.0	0.3	0.3
		trilobite cuticle indet.	NL	98.7	0.5	0.0	0.3	0.5
		trilobite cuticle indet.	NL	98.4	1.1	0.0	0.2	0.3
		trilobite cuticle indet.	NL	98.4	1.0	0.0	0.2	0.3
		trilobite cuticle indet.	NL	98.3	1.0	0.0	0.2	0.4
		trilobite cuticle indet.	NL	98.6	0.7	0.0	0.2	0.4
		trilobite cuticle indet.	NL	98.6	0.7	0.0	0.3	0.4
		trilobite cuticle indet.	NL	98.8	0.7	0.0	0.2	0.4
		ostracod indet.	L	98.6	0.9	0.0	0.3	0.3
		ostracod indet.	L	98.4	1.0	0.0	0.2	0.4
		ostracod indet.	L	98.4	0.9	0.0	0.3	0.4
		ostracod indet.	L	98.4	0.9	0.1	0.3	0.3
		sediment	NL	98.8	0.7	0.0	0.2	0.3
		sediment	NL	98.4	0.8	0.0	0.1	0.7
		sediment	NL	97.4	1.1	0.0	0.4	1.1
		sediment (dolomite)	NL	57.7	41.5	0.1	0.6	0.0
		calcite spar	L	98.7	0.6	0.0	0.3	0.4
		calcite spar	L	98.2	1.0	0.0	0.7	0.2
		calcite spar	L	98.4	1.0	0.0	0.6	0.0
		calcite spar	L	98.6	0.4	0.0	0.8	0.2
		calcite spar	L	98.9	0.5	0.0	0.4	0.1
1.1B	sp1	*Carolinites sibiricus* eye	NL	98.8	0.7	0.1	0.4	
	sp1	*Carolinites sibiricus* eye	NL	98.5	1.0	0.0	0.5	
	sp1	*Carolinites sibiricus* eye	NL	97.9	0.8	0.9	0.4	
	sp2	*Carolinites sibiricus* eye	L	97.8	1.8	0.1	0.3	
	sp2	*Carolinites sibiricus* eye	L	98.4	0.9	0.1	0.5	
		sediment	NL	98.6	0.8	0.1	0.6	
		calcite spar	L	98.2	1.3	0.1	0.4	
		calcite spar	L	97.8	1.9	0.0	0.3	
		calcite spar	L	98.0	1.7	0.0	0.3	
		calcite spar	L	98.6	1.0	0.1	0.4	
1.2C	sp1	*Carolinites genacinaca* eye	L	99.1	0.7	0.0	0.2	
	sp2	*Carolinites genacinaca* eye	L	98.9	0.6	0.0	0.3	0.2
		Carolinites genacinaca cuticle	NL	98.8	0.7	0.0	0.2	0.3
		Carolinites genacinaca cuticle	NL	98.6	0.7	0.1	0.3	0.3
		Carolinites genacinaca cuticle	NL	99.2	0.6	0.0	0.2	
		Carolinites genacinaca cuticle	NL	98.6	0.9	0.0	0.3	0.2
		Carolinites genacinaca cuticle	NL	98.2	1.3	0.0	0.3	0.3
		Carolinites genacinaca cuticle	NL	98.6	0.8	0.1	0.3	0.3
		Carolinites genacinaca cuticle	NL	98.7	0.9	0.0	0.2	0.2
		Carolinites genacinaca cuticle	NL	98.6	0.7	0.1	0.4	0.2
		Carolinites genacinaca cuticle	NL	98.9	0.6	0.0	0.4	0.1
		Carolinites genacinaca cuticle	NL	98.5	1.2	0.0	0.2	0.1
		Carolinites genacinaca cuticle	NL	98.4	0.9	0.0	0.4	0.3
		Carolinites genacinaca cuticle	NL	98.7	0.9	0.0	0.1	0.3
		Carolinites genacinaca cuticle	NL	99.0	0.5	0.0	0.3	0.2
		Carolinites genacinaca cuticle	NL	99.0	0.7	0.1	0.1	0.2
		Carolinites genacinaca cuticle	NL	99.0	0.6	0.0	0.2	0.1
		Carolinites genacinaca cuticle	NL	99.0	0.7	0.0	0.2	0.2
		Carolinites genacinaca cuticle	NL	98.7	0.9	0.0	0.2	0.2
		Carolinites genacinaca cuticle	NL	98.4	1.1	0.0	0.2	0.2
		Carolinites genacinaca cuticle	NL	98.7	1.0	0.0	0.2	0.1
		Carolinites genacinaca cuticle	NL	98.4	1.0	0.0	0.2	0.4

		Carolinites genacinaca cuticle	NL	98.5	1.0	0.0	0.2	0.3
		Carolinites genacinaca cuticle	NL	98.8	0.8	0.0	0.2	0.2
		Carolinites genacinaca cuticle	NL	98.9	0.7	0.0	0.2	0.2
		Carolinites genacinaca cuticle	NL	99.0	0.6	0.0	0.2	0.2
		sediment	NL	98.8	1.1	0.1	0.1	0.0
		sediment	NL	98.6	0.8	0.0	0.4	0.1
		sediment	NL	97.7	1.4	0.0	0.1	0.8
		sediment	NL	97.9	1.3	0.0	0.1	0.7
		calcite spar	L	98.7	0.7	0.0	0.3	0.2
		calcite spar	L	98.5	1.1	0.0	0.1	0.3
		calcite spar	L	99.0	0.9	0.0	0.1	0.1
		calcite spar	L	98.4	1.4	0.0	0.1	0.1
		calcite spar	L	98.7	0.4	0.1	0.4	0.3
		calcite spar	L	98.9	0.6	0.0	0.3	0.1
		calcite spar	L	99.0	0.7	0.0	0.3	0.0
		calcite spar	L	98.8	0.6	0.0	0.3	0.3
		calcite spar	L	98.9	0.7	0.0	0.2	0.2
		calcite spar	L	98.2	1.3	0.0	0.4	0.1
		calcite spar	L	98.3	1.1	0.0	0.2	0.3
		calcite spar	L	99.0	0.6	0.0	0.2	0.2
		calcite spar	L	98.8	0.8	0.0	0.2	0.2
		calcite spar	L	97.5	1.4	0.0	0.7	0.3
		calcite spar	L	98.9	0.5	0.0	0.3	0.3
		calcite spar	L	98.6	0.7	0.1	0.3	0.2
		calcite spar	L	98.7	0.7	0.1	0.2	0.3
		calcite spar	L	98.3	1.0	0.0	0.2	0.6
1.3		*Carolinites genacinaca* cuticle	NL	99.2	0.6	0.0	0.0	0.2
		Carolinites genacinaca cuticle	NL	99.3	0.6	0.0	0.0	0.1
		Carolinites genacinaca cuticle	NL	99.6	0.3	0.0	0.0	0.1
		Carolinites genacinaca cuticle	NL	99.5	0.5	0.0	0.0	0.0
		Carolinites genacinaca cuticle	NL	99.2	0.6	0.0	0.0	0.2
		calcite spar	L	99.3	0.6	0.0	0.1	0.1
		calcite spar	L	99.5	0.4	0.0	0.0	0.1
2.1B	sp1	*Carolinites genacinaca* eye	NL	98.1	1.9	0.0	0.0	
	sp1	*Carolinites genacinaca* eye	NL	98.2	1.7	0.0	0.1	
	sp1	*Carolinites genacinaca* eye	NL	99.2	0.8	0.0	0.0	
	sp1	*Carolinites genacinaca* eye	NL	98.5	1.2	0.1	0.1	
	sp1	*Carolinites genacinaca* eye	NL	99.1	0.9	0.0	0.0	
	sp2	*Carolinites genacinaca* eye	L	98.4	1.5	0.1	0.0	
	sp2	*Carolinites genacinaca* eye	L	98.6	1.3	0.1	0.1	
	sp2	*Carolinites genacinaca* eye	L	98.4	1.6	0.0	0.0	
	sp2	*Carolinites genacinaca* eye	L	99.4	0.6	0.0	0.0	
	sp2	*Carolinites genacinaca* eye	L	98.7	1.2	0.1	0.0	
		ostracod indet.	L	98.8	1.0	0.0	0.1	
		calcite spar	L	99.5	0.3	0.0	0.2	
		calcite spar	L	99.5	0.3	0.0	0.1	
		calcite spar	L	98.1	1.8	0.0	0.1	
		calcite spar	L	99.1	0.9	0.0	0.0	
		calcite spar	L	99.4	0.4	0.2	0.0	
		calcite spar	L	98.3	1.5	0.0	0.1	
		calcite spar	L	99.7	0.2	0.1	0.0	
2.2C		*Carolinites genacinaca* cuticle	n/a	98.5	1.4	0.0	0.2	
		Carolinites genacinaca cuticle	n/a	98.5	1.3	0.0	0.2	
		Carolinites genacinaca cuticle	n/a	97.4	2.3	0.1	0.2	
		Carolinites genacinaca cuticle	n/a	99.2	0.4	0.2	0.2	
		calcite spar	L	98.6	1.3	0.0	0.0	
2.4K		*Carolinites nevadensis* cuticle	NL	99.3	0.5	0.0	0.1	0.0
		Carolinites nevadensis cuticle	NL	99.4	0.4	0.1	0.0	0.1

		Carolinites nevadensis cuticle	NL	99.1	0.7	0.1	0.0	0.2
		sediment	NL	99.3	0.5	0.0	0.0	0.2
		sediment	NL	99.2	0.5	0.0	0.1	0.2
		sediment	NL	99.1	0.7	0.0	0.1	0.2
		sediment	NL	99.2	0.6	0.0	0.0	0.1
		sediment	NL	99.1	0.9	0.0	0.0	0.0
		calcite spar	L	97.9	1.3	0.5	0.1	0.3
		calcite spar	L	98.2	1.1	0.4	0.0	0.2
		calcite spar	L	98.2	0.9	0.4	0.0	0.4
		calcite spar	L	99.5	0.4	0.0	0.0	0.1
		calcite spar	L	99.4	0.4	0.0	0.0	0.2
		calcite spar	L	99.8	0.3	0.0	0.0	0.0
		calcite spar (vein)	L	98.2	1.0	0.5	0.1	0.3
		calcite spar (vein)	L	98.5	0.8	0.3	0.1	0.3
2.6	sp1	*Carolinites angustagena* eye (dolomitic)	NL	85.4	6.4	5.8	2.4	
	sp1	*Carolinites angustagena* eye (dolomitic)	NL	82.5	9.6	4.2	3.6	
	sp1	*Carolinites angustagena* eye (dolomitic)	NL	70.4	17.1	8.6	3.9	
	sp1	*Carolinites angustagena* eye (dolomitic)	NL	61.7	20.4	13.1	4.8	
	sp2	*Carolinites angustagena* eye	L	92.4	3.5	2.2	1.8	
	sp2	*Carolinites angustagena* eye	L	97.3	0.3	0.3	2.0	
	sp2	*Carolinites angustagena* eye (dolomitic)	NL	62.0	22.9	10.6	4.5	
	sp2	*Carolinites angustagena* eye (dolomitic)	NL	64.5	21.9	8.6	5.0	
	sp2	*Carolinites angustagena* eye (dolomitic)	NL	76.4	14.2	5.5	3.9	
	sp2	*Carolinites angustagena* eye (dolomitic)	NL	60.7	21.1	13.3	4.9	
		calcite spar	L	97.2	0.2	1.7	0.9	
		sediment	NL	97.4	0.1	1.5	1.0	

Electron microprobe results for the Valhallfonna Formation, reported as weight percent carbonate. Material examined at the University of Lille 1 was analyzed for wt% $SrCO_3$ while that examined at the University of Leicester was not. Abbreviations: Indet. = indeterminate species; CL = cathodoluminescence; L = luminescent; NL = non-luminescent, n/a = not applicable because the specimen was not analyzed.

Appendix C. Isotope results from dental drill, micro-mill and SIMS.

Sample	**Specimen**	**Species**	**Material**	**Method**	**d ^{13}C**	**d ^{18}O**	**Eye preservation**
			Vallhallfonna Formation, Spitsbergen				
0.1		Olenid indet.	cuticle	Dentist drill	-1.4	-8.5	
			sediment	Dentist drill	-1.6	-8.0	
0.2	C	*Carolinites genacinaca*	cuticle	Dentist drill	-0.3	-7.3	
			sediment	Dentist drill	-0.2	-6.3	
0.3	G	*Carolinites genacinaca*	cuticle	Dentist drill	-1.0	-8.0	
	G	*Carolinites genacinaca*	cuticle	Dentist drill	-0.4	-7.4	
			sediment	Dentist drill	-0.3	-7.4	
			sediment	Dentist drill	-0.3	-7.6	
			spar	Dentist drill	-0.4	-7.6	
0.4			sediment	Dentist drill	-1.2	-8.9	
			spar	Dentist drill	-1.9	-10.1	
1.1	A	*Carolinites sibericus*	eye	Dentist drill	-1.9	-8.6	poor
	B, sp1	*Carolinites sibericus*	eye	Dentist drill	-2.1	-9.8	poor
	B, sp1	*Carolinites sibericus*	lens	SIMS		-6.6	poor
	B, sp1	*Carolinites sibericus*	lens	SIMS		-7.6	poor

	B, sp1	*Carolinites sibericus*	lens	SIMS		-6.2	poor
	B	*Carolinites sibericus*	cuticle	Dentist drill	-1.2	-7.8	
	B	*Carolinites sibericus*	cuticle	Micro-mill	-0.9	-8.3	
	B	*Carolinites sibericus*	cuticle	Micro-mill	-0.8	-8.4	
	B		sediment	SIMS		-7.1	
	O	*Carolinites sibericus*	sediment	Dentist drill	-1.8	-8.0	
			sediment	Micro-mill	-1.0	-7.8	
			sediment	Dentist drill	-1.9	-8.2	
			sediment	Dentist drill	-1.3	-8.1	
			spar (vein)	Dentist drill	-2.3	-8.4	
			spar	Dentist drill	-1.1	-8.3	
			spar	Micro-mill	-1.0	-8.0	
1.2	C, sp1	*Carolinites genacinaca*	eye	Micro-mill	-0.1	-7.1	poor
			sediment	Micro-mill	-0.2	-6.7	
1.4			sediment	Dentist drill	-1.1	-9.0	
2.1	A	*Carolinites genacinaca*	cuticle	Dentist drill	-0.7	-7.1	
	A	*Carolinites genacinaca*	cuticle	Dentist drill	-0.4	-6.9	
	B, sp2	*Carolinites genacinaca*	lens	SIMS		-6.5	poor
	B, sp2	*Carolinites genacinaca*	lens	SIMS		-6.6	poor
	B, sp2	*Carolinites genacinaca*	lens	SIMS		-6.8	poor
	B, sp2	*Carolinites genacinaca*	Syntax. Cement	SIMS		-5.4	
		Olenid indet.	cuticle	Dentist drill	-0.4	-7.5	
			sediment	Dentist drill	-0.2	-7.8	
			sediment	Dentist drill	-0.0	-6.8	
			spar	Dentist drill	-0.7	-7.3	
2.2	C	*Carolinites genacinaca*	cuticle	Dentist drill	-0.9	-6.9	
	D	Olenid	cuticle	Dentist drill	-1.7	-7.4	
			sediment	Dentist drill	+0.3	-7.4	
			sediment	Dentist drill	+0.3	-7.6	
2.3	H	*Carolinites genacinaca*	cuticle	Dentist drill	-0.8	-7.1	
			sediment	Dentist drill	-0.4	-9.1	
			sediment	Dentist drill	+0.2	-7.5	
2.4	I	*Carolinites nevadensis*	eye	Dentist drill	-0.2	-7.2	
	I	*Carolinites nevadensis*	cuticle	Dentist drill	-0.6	-7.4	
	K	*Carolinites nevadensis*	cuticle	Dentist drill	-0.4	-7.3	
	M	*Carolinites nevadensis*	cuticle	Dentist drill	-0.3	-7.3	
			sediment	Dentist drill	-0.2	-7.3	
			sediment	Dentist drill	-0.3	-7.2	
			sediment	Dentist drill	-0.4	-7.3	
			sediment	Dentist drill	-0.3	-7.5	
2.5	E	*Carolinites* sp.	cuticle	Dentist drill	-0.9	-8.5	
			sediment	Dentist drill	-0.8	-7.6	
2.6	P_a	*Carolinites angustagena*	eye	Dentist drill	-1.1	-7.7	good
	P_b	*Carolinites angustagena*	eye	Dentist drill	-1.1	-7.6	good
	P	*Carolinites angustagena*	cuticle	Dentist drill	-1.4	-8.2	
	R	*Carolinites angustagena*	eye	Dentist drill	-1.2	-7.8	poor
		Carolinites angustagena	cuticle	Micro-mill	-1.1	-8.2	
		Carolinites angustagena	cuticle	Micro-mill	-1.7	-6.8	
		trilobite (unidentified)	cuticle	Dentist drill	-1.3	-7.9	
			sediment	Dentist drill	-1.2	-8.1	
			sediment	Dentist drill	-1.5	-8.0	
			sediment	Dentist drill	-1.2	-8.3	
			sediment	Dentist drill	-1.5	-7.2	
			sediment	Micro-mill	-1.2	-7.6	
			spar	Micro-mill	-1.6	-6.6	
			spar	Micro-mill	-1.4	-6.9	
2.7	T	*Carolinites* sp.	sediment	Micro-mill	-0.1	-7.1	
			sediment	Dentist drill	-0.6	-8.4	
			spar (vein)	Dentist drill	-1.6	-10.5	
			spar (vein)	Micro-mill	-2.7	-10.1	
			Emanuel Formation, Canning Basin, Australia				
705_159	A_159_sp1_a	Asaphid indet.	eye (half)	Micro-mill	-1.6	-7.7	good

	A_159_sp1_b	Asaphid indet.	eye (half)	Micro-mill	-2.3	-8.8	good
	A_159_sp1	Asaphid indet.	libriginae	Dentist drill	-1.7	-7.8	
	A_159_sp1		sediment	Dentist drill	-2.5	-8.0	
	A_159_sp1	Asaphid indet.	lens	SIMS		-8.4	good
	A_159_sp1	Asaphid indet.	lens	SIMS		-7.8	good
	A_159_sp1	Asaphid indet.	lens	SIMS		-8.1	good
	A_159_sp1		sediment	SIMS		-8.4	
	A_159_sp1	Asaphid indet.	libriginae	SIMS		-6.7	
	A_159_sp4	Asaphid indet.	libriginae	Dentist drill	-1.4	-7.8	
	A_159_sp4		sediment	Dentist drill	-1.3	-7.3	
705_178	A_178_sp1_a	Asaphid indet.	eye (half)	Micro-mill	-2.9	-7.5	good
	A_178_sp1_b	Asaphid indet.	eye (half)	Micro-mill	-3.1	-7.6	good
	A_178_sp1	Asaphid indet.	libriginae	Dentist drill	-3.0	-7.7	
	A_178_sp1	Asaphid indet.	lens	SIMS		-4.4	good
	A_178_sp1	Asaphid indet.	lens	SIMS		-5.0	good
	A_178_sp1	Asaphid indet.	lens	SIMS		-4.3	good
	A_178_sp1	Asaphid indet.	lens	SIMS		-4.2	good
	A_178_sp1	Asaphid indet.	lens	SIMS		-4.6	good
	A_178_sp1	Asaphid indet.	lens	SIMS		-4.7	good
	A_178_sp1	Asaphid indet.	libriginae	SIMS		-3.8	
	A_178_sp1	Asaphid indet.	libriginae	SIMS		-6.1	
	A_178_sp1		Syntax. Cement	SIMS		-4.6	
	A_178_sp1		sediment	SIMS		-4.7	
	T_178_sp1	*Opipeuterella* sp.	eye	Micro-mill	-3.9	-7.2	good
	T_178_sp1	*Opipeuterella* sp.	lens	SIMS		-6.9	good
	T_178_sp1	*Opipeuterella* sp.	lens	SIMS		-6.6	good
	T_178_sp1	*Opipeuterella* sp.	lens	SIMS		-6.3	good
	T_178_sp1	*Opipeuterella* sp.	lens	SIMS		-5.9	good
	T_178_sp1	*Opipeuterella* sp.	libriginae	SIMS		-6.4	
	T_178_sp1		Syntax. Cement	SIMS		-6.3	
	T_178_sp3	*Opipeuterella* sp.	eye	Micro-mill	-2.4	-8.3	poor
	T_178_sp3	*Opipeuterella* sp.	lens	SIMS		-5.3	poor
	T_178_sp3	*Opipeuterella* sp.	lens	SIMS		-4.7	poor
	T_178_sp3	*Opipeuterella* sp.	lens	SIMS		-4.8	poor
	T_178_sp3	*Opipeuterella* sp.	lens	SIMS		-4.6	poor
	T_178_sp3	*Opipeuterella* sp.	lens	SIMS		-4.9	poor
	T_178_sp3	*Opipeuterella* sp.	lens	SIMS		-4.9	poor
	T_178_sp3	*Opipeuterella* sp.	libriginae	SIMS		-7.0	
	T_178_sp3		sediment	SIMS		-8.4	
	T_178_sp4	*Opipeuterella* sp.	eye (sed contam.)	Micro-mill	-2.3	-8.5	poor
	T_178_sp4	*Opipeuterella* sp.	lens	SIMS		-2.8	poor
	T_178_sp4	*Opipeuterella* sp.	lens	SIMS		-3.9	poor
	T_178_sp4	*Opipeuterella* sp.	lens	SIMS		-2.4	poor
	T_178_sp4	*Opipeuterella* sp.	Cuticle	SIMS		-2.8	
	T_178_sp3 and 4	*Opipeuterella* sp.	libriginae	Dentist drill	-2.3	-9.1	
	T_178_sp3 and 4		sediment	Dentist drill	-1.5	-8.7	
	T_178_sp5	*Opipeuterella* sp.	libriginae	Dentist drill	-2.5	-8.0	
	T_178_sp5		sediment	Dentist drill	-1.7	-8.5	
	T_178_sp10	*Opipeuterella* sp.	eye	Micro-mill	-2.8	-7.7	good
	T_178_sp10	*Opipeuterella* sp.	lens	SIMS		-5.6	good
	T_178_sp10	*Opipeuterella* sp.	lens	SIMS		-4.0	good
	T_178_sp10	*Opipeuterella* sp.	lens	SIMS		-3.2	good
	T_178_sp10		Syntax. Cement	SIMS		-3.6	
	T_178_sp10		sediment	SIMS		-6.1	
705_205	A_205_sp1	Asaphid indet.	eye	Dentist drill	-2.1	-7.8	good
	A_205_sp1	Asaphid indet.	libriginae	Dentist drill	-2.7	-7.6	
	A_205_sp3	Asaphid indet.	eye	Micro-mill	-2.3	-7.6	poor
	A_205_sp3	Asaphid indet.	libriginae	Dentist drill	-2.5	-7.6	
	A_205_sp5	Asaphid indet.	eye	Micro-mill	-2.5	-7.7	good
	A_205_sp5	Asaphid indet.	libriginae	Dentist drill	-2.5	-7.5	
	A_205_sp5	Asaphid indet.	lens	SIMS		-9.3	good
	A_205_sp5	Asaphid indet.	lens	SIMS		-8.4	good

	A_205_sp5	Asaphid indet.	lens	SIMS		-10.4	good
	A_205_sp5		Syntax. Cement	SIMS		-10.1	
	A_205_sp5		sediment	SIMS		-10.4	
	A_205_sp10	Asaphid indet.	eye	Dentist drill	-2.7	-7.6	good
	A_205_sp10	Asaphid indet.	libriginae	Dentist drill	-2.4	-7.4	
	T_205_sp3	*Opipeuterella* sp.	eye	Micro-mill	-3.3	-7.2	good
	T_205_sp3	*Opipeuterella* sp.	libriginae	Dentist drill	-3.2	-7.7	
	T_205_sp3	*Opipeuterella* sp.	lens	SIMS		-7.6	good
	T_205_sp3	*Opipeuterella* sp.	lens	SIMS		-7.0	good
	T_205_sp3	*Opipeuterella* sp.	lens	SIMS		-8.0	good
	T_205_sp3		sediment	SIMS		-6.0	
	T_205_sp3		Syntax. Cement	SIMS		-7.1	
	T_205_sp4		sediment	Dentist drill	-2.8	-7.7	
			Horn Valley Siltstone Formation, Amadeus Basin, Australia				
84/3031/1	HV_sp2	Asaphid indet.	eye	Dentist drill	-1.1	-7.0	poor
	HV_sp2	Asaphid indet.	libriginae	Dentist drill	-2.2	-6.9	
	HV_sp2		sediment	Dentist drill	-1.7	-7.0	
	HV_sp6	Asaphid indet.	eye	Dentist drill	-3.3	-6.7	poor
	HV_sp6	Asaphid indet.	libriginae	Dentist drill	-3.0	-6.8	
	HV_sp20	Asaphid indet.	eye	Dentist drill	-1.7	-6.8	poor
	HV_sp20	Asaphid indet.	lens	SIMS		-5.2	
	HV_sp20	Asaphid indet.	lens	SIMS		-6.8	
	HV_sp20	Asaphid indet.	lens	SIMS		-5.4	
	HV_sp20	Asaphid indet.	lens	SIMS		-6.8	
	HV_sp20	Asaphid indet.	libriginae	SIMS		-6.9	
	HV_sp20		sediment	SIMS		-5.8	
84/3031/2	HV_sp4	*Carolinites genacinaca*	eye	Dentist drill	-2.3	-7.4	poor
	HV_sp5	*Carolinites genacinaca*	libriginae	Dentist drill	-1.9	-6.7	
	HV_sp5	*Carolinites genacinaca*	eye	Micro-mill	-2.0	-6.5	poor
	HV_sp27	Asaphid indet.	eye	Dentist drill	-1.6	-6.9	poor
	HV_sp27	Asaphid indet.	libriginae	Dentist drill	-2.2	-6.9	
	HV_sp37	*Carolinites genacinaca*	eye	Micro-mill	-1.8	-7.0	poor
	HV_sp43	*Carolinites genacinaca*	eye	Micro-mill	-2.0	-6.4	poor
	HV_sp43	*Carolinites genacinaca*	lens	SIMS		-4.2	poor
	HV_sp43	*Carolinites genacinaca*	lens	SIMS		-4.8	poor
	HV_sp43	*Carolinites genacinaca*	lens	SIMS		-5.0	poor
	HV_sp43	*Carolinites genacinaca*	lens	SIMS		-4.7	poor
	HV_sp43	*Carolinites genacinaca*	lens	SIMS		-4.1	poor
	HV_sp43	*Carolinites genacinaca*	lens	SIMS		-4.0	poor
	HV_sp43	*Carolinites genacinaca*	lens	SIMS		-6.3	poor
	HV_sp43	*Carolinites genacinaca*	lens	SIMS		-6.3	poor
	HV_sp43	*Carolinites genacinaca*	lens	SIMS		-3.6	poor
	HV_sp43	*Carolinites genacinaca*	libriginae	SIMS		-6.4	
	HV_sp43		Syntax. Cement	SIMS		-5.6	
	HV_sp94	*Carolinites genacinaca*	eye	Dentist drill	-1.6	-6.5	poor

Isotope results for three of the isotope extraction methods used; hand extraction of multiple lenses using a dental drill and the automated extraction of multiple lenses by micro-mill were tested using conventional isotope analysis. The automated analysis of individual eye lenses was undertaken using SIMS analysis (giving $\delta^{18}O$ only). Specimens with a preservation assignment were analyzed in thin section or as whole specimens where internal structures were revealed on the SEM. Abbreviations: The suffix ‘a’ and ‘b’ after the specimen name indicates that two areas of the same eye were drilled on the micro-mill, to give two

different isotope results. Indet. = indeterminate species of a particular trilobite family. Librigena refers to the cheek region of the trilobite cuticle that was drilled next to the eye.

Appendix D. Carbonate clumped isotopes results

Sample	Formation	Material	carbonate $\delta^{13}C$ (‰, PDB)	carbonate $\delta^{18}O$ (‰, PDB)	$\Delta_{47CDES25}$ ‰, CDES	Estimated T°C from Δ_{47}	Reconstructed $\delta^{18}O$water (‰, SMOW)
0.4_run1	Valhallfonna Fm	sediment	0.14	-8.51	0.589		
0.4_run2	Valhallfonna Fm	sediment	0.09	-8.53	0.587		
0.4_average	Valhallfonna Fm	sediment	0.12	-8.52	0.588	65	0.0
0.4_run1	Valhallfonna Fm	cuticle indet. (combined)	-0.75	-8.11	0.571		
0.4_run2	Valhallfonna Fm	cuticle indet. (combined)	-0.69	-8.03	0.590		
0.4_average	Valhallfonna Fm	cuticle indet. (combined)	-0.72	-8.07	0.581	68	1.0
1.2	Valhallfonna Fm	cuticle indet. (combined)	-0.51	-7.46	0.610	55	-0.4
705_178	Emanuel Fm	sediment	-2.81	-7.41	0.608	56	-0.2
705_178_run1	Emanuel Fm	Asaphid indet. Cuticle	-2.77	-7.44	0.614		
705_178_run2	Emanuel Fm	Asaphid indet. Cuticle	-2.78	-7.35	0.612		
705_178_average	Emanuel Fm	Asaphid indet. Cuticle	-2.77	-7.39	0.613	54	-0.6
705_205	Emanuel Fm	sediment	-1.45	-7.75	0.623	50	-1.6
705_205_run1	Emanuel Fm	Asaphid indet. Cuticle	-2.39	-7.44	0.618		
705_205_run2	Emanuel Fm	Asaphid indet. Cuticle	-2.38	-7.38	0.626		
705_205_average	Emanuel Fm	Asaphid indet. Cuticle	-2.39	-7.41	0.622	50	-1.2
705_205_run1	Emanuel Fm	cuticle indet.	-2.89	-7.37	0.623		
705_205_run2	Emanuel Fm	cuticle indet.	-2.86	-7.39	0.615		
705_205_average	Emanuel Fm	cuticle indet.	-2.88	-7.38	0.619	51	-1.0
3031/2	Horn Valley Siltstone	sediment	-1.7	-7.16	0.608	56	0.0
3031/2_run1	Horn Valley Siltstone	Asaphid indet. Cuticle	-2.18	-6.71	0.611		
3031/2_run2	Horn Valley Siltstone	Asaphid indet. Cuticle2	-2.15	-6.7	0.602		
3031/2_average	Horn Valley Siltstone	Asaphid indet. Cuticle3	-2.17	-6.71	0.606	57	0.6
Västergötland1	Upper Mb Dalby Lst	sediment	-0.03	-7.12	0.396	214	na
Västergötland2	Upper Mb Dalby Lst	*Telephina* cuticle	-0.38	-5.94	0.383	233	na

Δ_{47} results from trilobite cuticle and rock sediment from four different formations. Cuticle was extracted from asaphid specimens, one specimen of *Telephina* and indeterminate specimens. $\Delta_{47\ CDES25}$ are given in ‰ in both the Carbon Dioxide Equilibrated Scale as named by Henkes et al. (2013) – that corresponds to a

direct transfer into the absolute reference frame described by Dennis et al. (2011) – and in the 25°C acid digestion reference frame. Oxygen and carbon isotopic compositions of the carbonate (carbonate $\delta^{18}O$ and $\delta^{13}C$) are given in ‰ relative to the PDB scale while the oxygen isotopic composition of the water from which the carbonate precipitated ($\delta^{18}O_{water}$) are reported in ‰ variations relative to the SMOW scale. Replicate measurements of the same sample (i.e. repeat of the whole extraction, purification and analysis procedures) are indicated by the suffix _run1 or _run2. All samples were analyzed over a time period of one year with unknown samples interspersed with CO_2 gases equilibrated at both 25 and 1000°C together with carbonate reference materials GCAZ-01b and Carrara marble (both analyzed in Dennis et al., 2011, for defining the absolute reference frame and several other papers afterwards; e.g., Bonifacie et al., 2016). Note that though triplicate Δ_{47} measurements are usually recommended to attain optimal accuracy and precision on Δ_{47} values (close to ± 0.008‰), and thus associated temperature estimates, the very good consistencies for both replicate Δ_{47} measurements of the same powder and/or Δ_{47} values found for various samples from the same formation, indicate that all carbonate samples from the same formation recrystallized at comparable temperatures.